Direct estimates of the Indonesian Throughflow entering the Indian Ocean: 2004-2006

Janet Sprintall, Susan E. Wijffels, Robert Molcard, Indra Jaya

Direct estimates of the Indonesian Throughflow entering the Indian Ocean: 2004–2006

Janet Sprintall,[1] Susan E. Wijffels,[2] Robert Molcard,[3] and Indra Jaya[4]

Received 23 December 2008; revised 6 April 2009; accepted 4 May 2009; published 1 July 2009.

[1] The mean and variable transport of the Indonesian Throughflow (ITF) are determined from full-depth velocity measurements in the three major exit passages of Lombok Strait, Ombai Strait, and Timor Passage from January 2003 through December 2006. Collectively, these passages convey the full-depth transport and stratification profile of the ITF from the Pacific Ocean to the Indian Ocean. To first order, the seasonal cycle of transport in the thermocline (~100–150 m) in all three exit straits is dominated by regional monsoon forcing, with maximum ITF during the southeast monsoon. During the northwest monsoon, the surface transport relaxes in Timor and weakly reverses in Ombai and Lombok, so the main core of the ITF is subsurface. Below the thermocline, semiannual reversals occur in all three straits during the monsoon transitions in response to the passage of Indian Ocean wind-forced Kelvin waves. However, the reversals occur over different depth levels in each passage reflecting the influence of different sill depths along the coastal waveguide. The seasonal cycle of depth-integrated transports in Lombok and Ombai are strongly out of phase with Timor Passage, suggesting that the subthermocline flow is largely gated by these Kelvin waves. Despite the different seasonal transport phases, interannual anomalies in all three passages are remarkably similar, particularly during the strong positive Indian Ocean Dipole event in 2006 when transport in the surface layer is toward the Indian Ocean and reversed below. The deep reversals are likely in response to a series of Kelvin waves driven by anomalous zonal winds in the equatorial Indian Ocean. Total mean transport over the 3-year period is −2.6 Sv in Lombok Strait (i.e., toward the Indian Ocean), −4.9 Sv in Ombai Strait, and −7.5 Sv in Timor Passage. The transport in Timor Passage is nearly twice as large as historical estimates and represents half of the −15 Sv full-depth ITF transport that enters the Indian Ocean.

Citation: Sprintall, J., S. E. Wijffels, R. Molcard, and I. Jaya (2009), Direct estimates of the Indonesian Throughflow entering the Indian Ocean: 2004–2006, *J. Geophys. Res.*, *114*, C07001, doi:10.1029/2008JC005257.

1. Introduction

[2] The Indonesian seas are the only major low-latitude connection in the global oceans. This connection permits the transfer of Pacific waters into the Indian Ocean, known as the Indonesian Throughflow (ITF). The ITF actually consists of several filaments of flow that occupy different depth levels and weave their way through the complex island geometry comprised of broad shallow shelves and deep basins. The largest Indonesian seas are (from west to east): the shallow Java Sea, the deeper Flores, Banda and Timor Seas, and the shallow Arafura Sea (Figure 1a).

[3] Surface to upper thermocline waters, drawn primarily from the North Pacific, take the "western" route through the Sulawesi Sea into Makassar Strait. Within Makassar Strait, the 680 m deep Dewakang sill permits only the upper thermocline waters to enter the Flores Sea and flow eastward to the Banda Sea, or to directly exit into the Indian Ocean via the shallow (300 m) Lombok Strait. Smaller contributions of North Pacific surface water may also take an "eastern" route through the Maluku Sea and over the deeper (1940 m) sill of Lifamatola Strait into the Banda Sea. Lower thermocline and intermediate water masses of South Pacific origin also enter the Indonesian seas via an eastern route. The denser South Pacific water masses are distinctly saltier than the North Pacific upper waters. Within the Banda Sea, these water masses are modified by tidally forced mixing, wind-driven upwelling, and surface heat and freshwater fluxes to form the distinctive Indonesian sea profile of relatively isohaline water from the thermocline to near bottom [*Ffield and Gordon*, 1992; *Bray et al.*,

[1] Scripps Institution of Oceanography, University of California San Diego, La Jolla, California, USA.
[2] Centre for Australian Weather and Climate Research, Commonwealth Scientific Industrial Research Organization Marine and Atmospheric Research, Hobart, Australia.
[3] Laboratoire d'Oceanographie et du Climat: Experimentation et Approaches Numeriques, Université Pierre et Marie Curie, Paris, France.
[4] Department of Marine Sciences and Technology, Bogor Agricultural University, Bogor, Indonesia.

0148-0227/09/2008JC005257

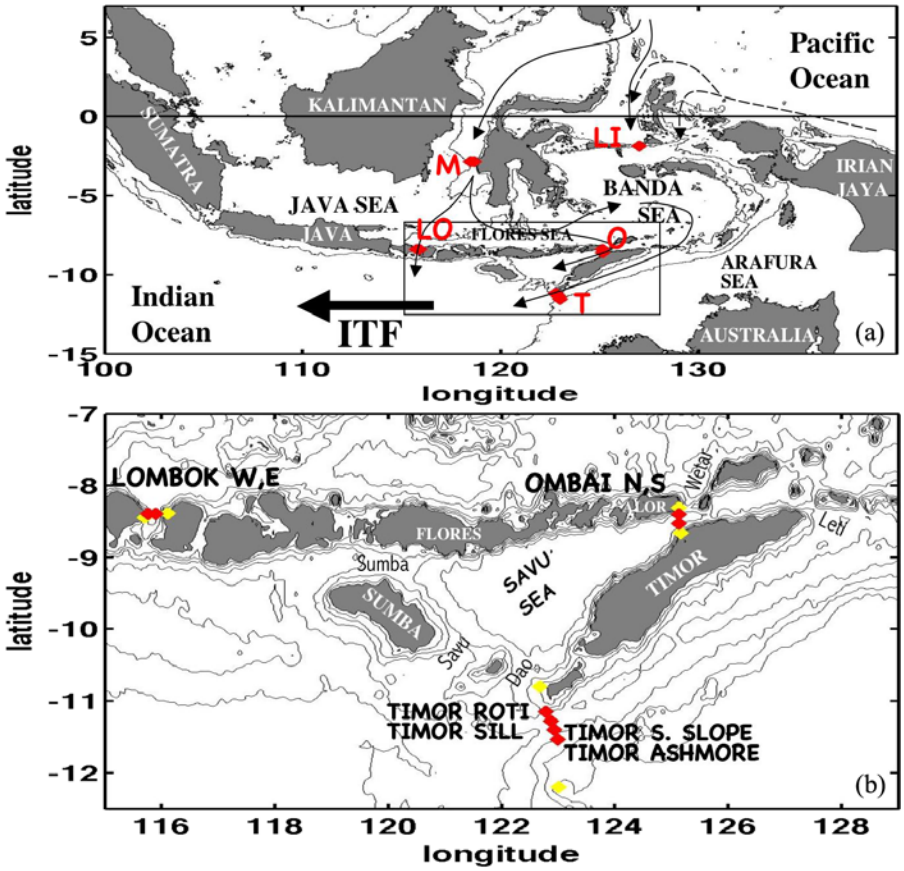

Figure 1. (a) The Indonesian Seas and schematic of the pathways of the Indonesian Throughflow (ITF). The location of INSTANT moorings deployed in Makassar Strait (M), Lifamatola Strait (LI), Lombok Strait (LO), Ombai Strait (O), and Timor Passage (T) are shown as red diamonds. (b) The boxed inset shows the location of the INSTANT moorings (red diamonds) and shallow pressure gauges (yellow diamonds) deployed in the exit passages along Nusa Tenggara, showing the 200, 500, 1000 (also in Figure 1a), 2000, and 4000 m isobaths.

1996; *Hautala et al.*, 1996; *Waworuntu et al.*, 2000; *Koch-Larrouy et al.*, 2008].

[4] From the Banda Sea, the ITF exits into the southeast Indian Ocean along the Nusa Tenggara island chain (Figure 1b) via the Timor Passage (1250 m eastern sill depth at Leti Strait, and 1890 m at the western end), or through Ombai Strait (upstream sill depth of 1450 m in Alor Strait and 2450 m in Wetar Strait) and then through the Savu Sea to Sumba Strait (900 m) or Savu/Dao Strait (1150 m). Other passages along the Nusa Tenggara archipelago are too shallow (<50 m) to significantly contribute to the ITF mass transport, and the flow through these channels is dominated by tidal and/or frictional forces [*Godfrey*, 1996; *Hautala et al.*, 2001; *Wijffels et al.*, 2008]. From the major exit passages, the ITF waters form a relatively narrow fresh jet across the entire tropical South Indian Ocean between 8°S to 14°S within the westward-flowing South Equatorial Current (SEC). Recognizable across the entire basin, the ITF waters form a distinct low salinity core of surface to thermocline water [*Gordon et al.*, 1997] and a separate salinity minimum/silica maximum core at intermediate depths (600–1200 m [*Talley and Sprintall*, 2005]). At the western edge of the Indian Ocean, while some ITF waters feed the monsoon currents off the Somali coast, it is likely that much of the ITF enters the Agulhas Current system [*Warren*, 1981; *You*, 1998], and numerous Agulhas eddies in the Atlantic have been identified as containing relatively fresh Indonesian thermocline water [*Gordon*, 1986; *Song et al.*, 2004]. This evidence supports the numerical models [e.g., *Hughes et al.*, 1992; *Hirst and Godfrey*, 1993, 1995; *Schiller et al.*, 1998; *Lee et al.*, 2002] that show the ITF plays an important role in the global thermohaline circulation. The ITF also likely impacts the global atmospheric circulation via its modification of tropical surface temperature patterns as shown by the coupled modeling work of *Schneider* [1998]. The impact of the ITF in the coupled system depends on its magnitude, heat flux and variability, which have yet to be thoroughly constrained by observations.

[5] Past estimates of the mean ITF mass transport are based on both synoptic and time-averaged, direct and indirect methods, and are thus wide ranging from near zero to 30 Sv (1 Sv = 10^6 m^3s^{-1} [*Godfrey*, 1996]). Direct measurement of the flow and properties within the exit passages, that when combined represent the full ITF and its stratification, have only been obtained at different times in the different channels over the past few decades (Table 1). To date, our best estimate of the total ITF transport through the exit passages is probably around 10–14 Sv although,

Table 1. Comparison of the Mean ITF Transport Estimates and Uncertainties (Sv, Negative Toward Indian Ocean) During the INSTANT Field Program (2004–2006 Averages) With Previously Published Transport Values for Each Exit Passage[a]

Strait	Reference	Time Period Average	Total Transport (Sv)	Transport Uncertainty (Sv)	Depth Range (m) Width (km)
Lombok	*Murray and Arief* [1988]	1985	−1.7	±1	0–300 m
	INSTANT	2004–2006	−2.6	−1.8 to −3.2	0–300 m 35 km
Ombai	*Molcard et al.* [2001]	1996	−5.0	±1	0–1250 m
	INSTANT	2004–2006	−4.9	−2.7 to −5.0	0–1200 m 35 km
Timor	*Cresswell et al.* [1993]	1984/1985 and 1988	−7	N/A	0-bottom 160 km
	Molcard et al. [1994]	1989	−4.5	±1.5	120–1040 m
	Molcard et al. [1996]	1992	−4.3	±1.0	0–1250 m 85 km
	INSTANT	2004–2006	−7.5	−6.2 to −10.5	0–1890 m 160 km
TOTAL ITF	INSTANT	2004–2006	−15.0	−10.7 to −18.7	sill depth and width as indicated above

[a]Uncertainties during the INSTANT time period are given as a range of minimum and maximum transport values depending on the schemes used for the surface layer and across-passage interpolation (see text for details). For uncertainties associated with previous published values, see associated reference. Total transport during INSTANT is also given.

because of the different sampling years of the different direct measurement programs, this total volume transport estimate should be treated with caution. There are no estimates of the heat or freshwater transports for the full exit flow. Furthermore, the variability of the volume and properties of the ITF is the same order as the mean, which has a substantial impact on the transport estimates from a given passage in a given year. Only with multiyear, simultaneous measurements of the full-depth velocity structure in all the major Throughflow passages can the volume and property transports be accurately determined.

[6] To obtain a complete multiyear ITF transport estimate, an array of 11 moorings were deployed as part of the International Nusantara Stratification and Transport (INSTANT) program [*Sprintall et al.*, 2004]. The moorings were deployed simultaneously over a ~3-year period in the two major inflow passages of Makassar and Lifamatola Straits, and in the three major outflow passages of Lombok, Ombai and Timor (Figure 1). The mooring array was designed to measure the full depth *in situ* velocity, temperature and salinity profiles of the ITF. INSTANT observations in Makassar Strait are discussed by *Gordon et al.* [2008] and in Lifamatola Strait in *van Aken et al.* [2009]. In this paper, we discuss the mean and variability of the transport through the three major outflow passages of Lombok, Ombai and Timor, which collectively capture the full interbasin exchange. Our focus is the vertical structure and properties of the complete ITF, the relative partitioning of the transport through these three straits, and how this changes on subinertial, seasonal and interannual timescales. The INSTANT measurements reveal a number of new, major features of the ITF that have been previously undocumented and are highlighted in this manuscript: a semipermanent reversal of the flow in northern Ombai Strait that permits Indian Ocean water into the internal Banda Sea to participate in the formation of Indonesian Throughflow Water; the relatively small amplitude of the seasonal cycle in total transport; the first documented time series of Indonesian Intermediate Water simultaneously in Ombai and Timor straits; and a comparatively similar response of the interannual transport anomalies in all three exit passages to the 2006 Indian Ocean Dipole. Our best estimate of the total transport from the three exit passages into the Indian Ocean is −15 Sv, which is slightly more than that estimated from previous direct measurements of the ITF.

2. The INSTANT Mooring Data

2.1. Mooring Deployments and Instrumentation

[7] The first INSTANT mooring was deployed in East Timorese waters in southern Ombai Strait in August 2003 from the Australian vessel *R/V Southern Surveyor*. The seven other outflow passage moorings were deployed using the Indonesian vessel, the *KR Baruna Jaya VIII*, in December 2003–January 2004. The location and depth of deployment of each mooring is given in Table 2. Besides the need for redundancy in case of a mooring failure in these tidally dynamic, heavily fished passages, multiple mooring deployments were made in each strait to partly resolve the distinct cross-passage flow structure evident from some

Table 2. Exit Strait Sill Depth, Width Used for Transport Calculation, and the Location, Depth, and Deployment Periods for Each Mooring in That Strait[a]

Strait	Mooring	Location	Depth (m)	Deployment Period
Lombok Strait Sill: 300 m	east	115°53.88′E 8°24.14′S	1144	10 January 2004–16 December 2006
Width: 35 km	west	115°45.55′E 8°26.39′S	921	9 January 2004–15 June 2005
Ombai Strait Sill: 3250 m	north	125°0.16′ E 8°24.10′ S	1329	4 January 2004–6 December 2006
Width: 35 km	south	125°3.86′E 8°32.00′S	3224	8 August 2003–7 December 2006
Timor Passage Sills: 1250 m (Leti)	roti	122°46.79′ E 11°09.75′ S	741	1 January 2004–13 December 2006
1890 m (West Timor)	sill	122°51.90′ E 11°16.48′ S	1890	31 December 2003–12 December 2006
Width: 160 km	south slope	122°57.59′ E 11°22.09′ S	1386	30 December 2003–12 December 2006
	Ashmore	122°58.44′ E, 11°31.70′ S	902	30 December 2003–13 December 2006

[a]The location and depth of each mooring is given for the first 18-month deployment period (December 2003–June 2005) and are very similar to the redeployment positions for the second 18-month deployment (June 2005–December 2006). The top part of the Timor Sill mooring from deployment 1 prematurely parted in August 2004, but this instrumentation and a deeper current meter were later recovered during the turn-around cruise in June 2005. The Lombok West mooring was not recovered for the second deployment period.

tidally averaged shipboard Acoustic Doppler Current Profiler (ADCP) surveys described by *Hautala et al.* [2001]. Coastal shallow pressure gauges were also deployed on either side of each exit passage to directly measure the sea level slope for proxy surface geostrophic transport calculations, and the mooring locations in each passage were located along a line between the pressure gauges (Figure 1).

[8] Lombok Strait is 35 km wide, and the two moorings (Lombok West and Lombok East) were deployed in deeper water north of the ~300 m sill, as the currents at the sill are too strong to deploy a tall mooring. Lombok is the outflow portal for the Makassar Jet, with perhaps a smaller contribution from the South China Sea by way of Karimata Strait in the Java Sea [*Tozuka et al.*, 2007]. Lombok is also the first major passage along Nusa Tenggara that is exposed to flow from the equatorial Indian Ocean (Figure 1). Ombai Strait is 37 km wide across the ~3250 m basin where two moorings (Ombai North and Ombai South) were deployed between the pressure gauges. The southern mooring site is the same as that instrumented by *Molcard et al.* [2001]. Net flow through Ombai is constrained downstream by Sumba Strait (~900 m) and Savu/Dao Strait (~1150 m). Timor Passage is the widest exit strait, being 160 km wide at the western sill where four moorings were deployed (Timor Roti, Timor Sill, Timor South Slope, and Timor Ashmore). Below 1250 m depth, corresponding to the upstream Leti sill at its eastern edge, the Timor Basin is isolated from the Banda Sea but connected to the Indian Ocean down to 1890 m (depth of the western sill instrumented by INSTANT). A significantly wide but shallow continental shelf, the Australian Northwest Shelf, is located to the south of Ashmore Reef (Figure 1). Like the Java Sea shelf, flow across this shelf was not monitored during INSTANT, although earlier surveys by *Cresswell et al.* [1993] suggested that its net contribution to the interocean exchange is small. Thus we believe that the INSTANT array across the three exit passages captures nearly all the interbasin exchange.

[9] All 8 moorings in the exit passages were recovered, refurbished and redeployed in June–July 2005 from the *KR Baruna Jaya VIII*. The upper section (surface to 1400 m) of the Timor Sill mooring had parted in August 2004, but the instrumentation was recovered providing a ~7 month record. In addition, two deeper current meters were recovered during the July 2005 turn-around cruise and provided a full 18-month deployment record below 1400 m at the Timor Sill. Final recovery of all moorings occurred in December 2006 from the *KR Baruna Jaya I*, except for the Lombok West mooring which parted a month earlier and went missing.

[10] Mooring velocity instrumentation configuration was fairly similar on all moorings (see Figure 3), with an upward-looking ADCP deployed so as to resolve the surface to thermocline flow, and single-point current meters positioned at depth to resolve the subthermocline to intermediate depth flow. The ADCPs and most current meters included temperature and pressure sensors, and additional temperature, temperature-pressure and temperature-salinity-pressure sensors were deployed at discrete depths throughout the water column. Sampling rates were set to resolve the tides, and varied between 10 minutes through to 2 hours for the deeper current meters. As anticipated, pressure time series revealed that all moorings were subjected to substantial blow-over through tidal and low-frequency forcing, with moorings typically profiling 50–100 m at peak tides (though South Ombai mooring profiled > 300 m). For each instrument without a direct pressure measurement or with gaps, pressure was assigned using the nearest full time series pressure record and the planned deployment wire lengths between instruments. Complete details of all mooring instrumentation, deployment depths, data coverage and the quality control for treatment of compass errors, time drifts, and fouling can be found in the online data report [*Cowley et al.*, 2008].

2.2. Handling Data Gaps

[11] After quality control of the individual instrument records, a data set for each mooring was compiled by "stacking" filtered and interpolated data onto a common time base of 1 hour. The velocity data were then vertically linearly interpolated onto a 10-m-depth grid for each hour time step. In order to estimate transport errors associated with missing velocities in the surface layer (typically the upper 30–50 m due to surface reflection contamination of the ADCP), gaps were filled using three models: (1) a constant velocity equal to the shallowest measured velocity (i.e., a "slab" extrapolation), (2) constant shear to the surface, and (3) extrapolation to zero velocity. Similarly, the missing velocity at the ocean bottom needs to be accounted for in the transport calculations. In Lombok and Ombai Straits, the velocity is assumed to be zero at the bottom, because the moorings in these straits were deployed at depths much greater than the controlling sill depths of 300 m and 1150 m, respectively. In Timor Passage the moorings were deployed on the sill exposed to the Indian Ocean, so for these moorings both a slab approach assigning the deepest measured velocity to the missing data below, and a constant shear to zero velocity at the bottom assumptions were used.

[12] The vertically gridded velocity time series was then low-pass filtered with a 4-day Hamming window (to suppress the inertial and tidal variability) and subsampled to daily values. Finally, the Cartesian velocities were rotated based on the orientation of the pressure gauges (Lombok 350°T; Ombai 80°T; Timor 246°T) into along strait velocities (ASV).

[13] Significant gaps in the ASV time series occur for the Timor Sill data: from the surface to 1400 m depth from August 2004 to June 2005 during deployment 1 due to the mooring parting early; and during deployment 2 the ADCP had a faulty connection and only a small number of bins close to the instrument were retrieved. The second deployment of Timor Ashmore failed to release and was trawled up leaving a data gap below 400 m. In addition, the second mooring deployment of Lombok West from June 2005–December 2006 was not recovered. These gaps, along with shorter gaps due to individual instrument failure, were filled by finding predictors for the missing ASV using the available temperature and ASV data from the surrounding moorings. That is, the ASV at each depth was expressed as a linear combination of predictors whose coefficients were determined using a damped least squares fit; the predictors were the normalized temperature and ASV from the surrounding moorings at all available depths. As in all damped least squares solutions, results are sensitive to the assumed

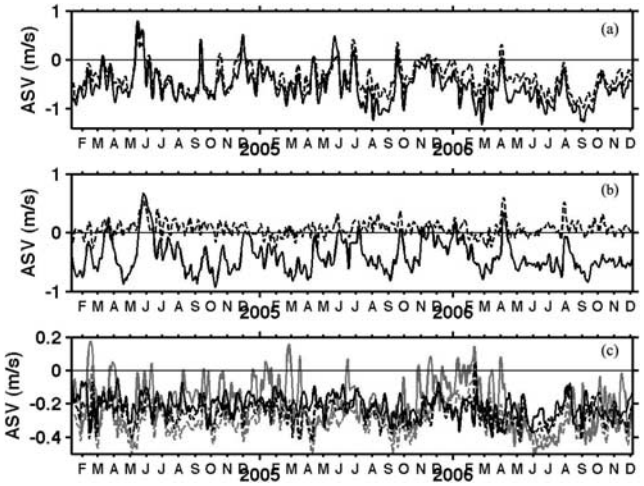

Figure 2. Time series of the along-strait velocity (ASV, m s^{-1}) at 100-m depth measured at the INSTANT moorings (a) Lombok West (solid) and Lombok East (dashed); (b) Ombai South (solid) and Ombai North (dashed); and (c) Timor Ashmore (black solid), Timor South Slope (black dashed), Timor Sill (gray dashed), and Timor Roti (gray solid). Note different velocity scales in each panel.

ratio between the solution size and the residual size. An independent test of the accuracy of each prediction was to reduce the size of the training data set (the available ASV observations) and then compare predictions for the withheld data. Residuals between the observed and the predicted ASV were typically found to be ~0.05–0.10 m s^{-1}, and the predictor errors are believed small compared to other interpolation errors (see below). The resulting predicted ASVs were then used to fill the gaps in the time series.

2.3. Cross-Passage Interpolation of Velocity

[14] To estimate the transport through each strait, the mooring point observations need to be laterally interpolated between the moorings and extrapolated to the strait sidewalls. Our choices were guided by earlier available mooring and shipboard ADCP data in each strait; remotely sensed color and SST data; and the cross-passage differences evident in the flow from the moorings themselves.

[15] In Lombok Strait, the two moorings are separated by 15.8 km, and the ASV toward the Indian Ocean was slightly stronger at Lombok West compared to Lombok East (Figure 2a), as also observed during three snap-shot shipboard ADCP surveys by *Hautala et al.* [2001]. There is a very strong correlation between ASV at Lombok East and West at all depths above the sill (a result also confirmed through the least squares prediction used to fill the missing second deployment Lombok West data). In contrast to Lombok, the ASV at Ombai North is completely different from that at Ombai South (Figure 2b), even though these two moorings are separated by only 14.7 km. The strongest ITF is primarily confined to the southern part of the strait, although upper layer reversals are equally strong in both Ombai North and South. The ADCP surveys across Ombai Strait reported by *Hautala et al.* [2001] also show the strongest westward Throughflow is mainly confined to the southern two thirds of the strait. Persistent strong midstrait surface fronts are evident in ocean color, SST and Synthetic Aperture Radar imagery [e.g., *Moore and Marra*, 2002], and these express different flow dynamics on either side of Ombai Strait. In both Lombok and Ombai Straits, the shipboard ADCP transects show significant flow up to a kilometer or so from the coast, suggesting that the sidewall boundary is very narrow. Compared to Lombok and Ombai, the flow at all 4 moorings in Timor Passage is relatively steady toward the Indian Ocean (Figure 2c), with reversals most common at the northern-most Timor Roti that are often out of phase with ASV at the southern Timor Ashmore, possibly indicating the presence of clockwise rotating eddies passing through this strait [*Feng and Wijffels*, 2002].

[16] Based on this information, three schemes were chosen for possible cross-passage interpolation (in 1 km bins) of the mooring ASV data in each of the three exit passages: (1) linear interpolation across the passage (referred to in the following as linear), (2) cubic-spline interpolation across the passage (cubic) and (3) evenly dividing the cross-passage distance between the moorings with ASV uniformly assigned by the nearest mooring (block). In all schemes, zero flow is assumed in the last 1 km bin nearest the sidewalls, suggesting an effective channel width that is slightly less than the topographic width. A fourth scheme was also chosen for Lombok and Ombai to allow for the observed flow intensification horizontally across these passages: (4) dividing the cross-passage with a frontal boundary at 115.8°E in Lombok and 8.4°S in Ombai, with ASV uniformly assigned by the nearest mooring, assuming zero flow in the last 1 km bin nearest the sidewalls (w-block). A stationary position was chosen to mimic the front because unfortunately the remotely sensed SST and color images are significantly impacted by cloud in this monsoonal region and hence a complete time series is not available. In all transport schemes we used the *Smith and Sandwell* [1997] 30-arc second bathymetry to determine the strait area.

[17] Figure 3 shows the ASV mean and standard deviation for the 3-year time series using the constant shear surface model and cubic-spline interpolated across the channel with a no slip condition at the sidewalls. Each exit passage is displayed down to the sill depth of relevance for exchange between the Pacific and Indian Ocean, and the sign convention to be used in this paper is such that negative flow is into the Indian Ocean (i.e., the ITF). Western intensification is evident in Lombok Strait with this side of the channel also exhibiting the most variability (Figure 3a). The mean above sill flow in Lombok is all directed toward the Indian Ocean.

[18] A major new result from the INSTANT measurements is the nature of the flow on the northern side of Ombai where the flow is directed *away* from the Indian Ocean and toward the internal seas (Figure 3b). A surface core extending to ~80 m depth, with mean flows of ~0.10–0.17 m s^{-1}, is separated by a region of weak flow toward the Indian Ocean from a deeper eastward core that hugs the coastline between ~220 and 800 m depth. We believe that these two cores are eastward extensions of the surface South Java Current (SJC) and the subsurface South Java Undercurrent (SJUC). These currents are found with a near identical vertical structure near the coast of Java in the annual geostrophic velocity mean from the XBT transect IX1 data [*Meyers et al.*, 1995; *Wijffels et al.*, 2008], from

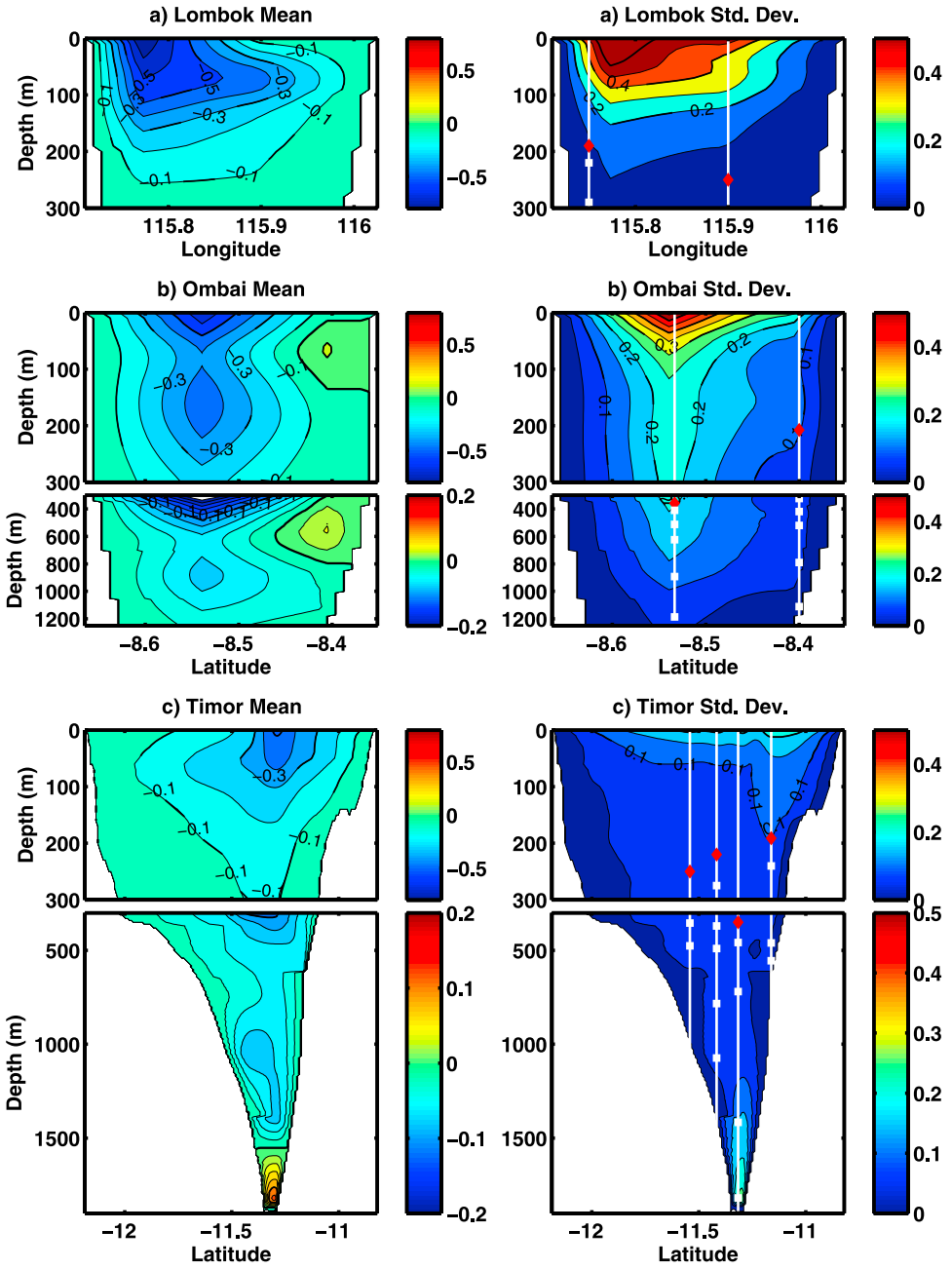

Figure 3. (left) Mean and (right) standard deviation of the along-strait velocity in (a) Lombok Strait, (b) Ombai Strait, and (c) Timor Passage to the respective sill depths. Note the change in depth scales below 300 m in Ombai and Timor. The position of the moorings across each passage and velocity instrumentation (diamonds, ADCP; squares, discrete current meters) is shown schematically overlain in white.

various synoptic CTD surveys south of Java and Bali [*Fieux et al.*, 1994, 1996; *Wijffels et al.*, 2002], and the synoptic velocity sections of the study by *Hautala et al.* [2001]. Salty intermediate water suggesting an intrusion of North Indian Intermediate Water carried by the SJUC has also been identified from INSTANT cruise CTD data [*Atmadipoera et al.*, 2009]. The presence of the lateral reversal in the northern part of Ombai Strait strongly supports the idea that the SJC and the SJUC are sustained by Indian Ocean wind-driven Kelvin wave energy, which is therefore confirmed to extend past Lombok and Sumba Strait and onto Ombai. In southern Ombai Strait, two ITF cores are evident: a surface core with flow dropping to a minimum near ∼80 m depth and a slightly stronger subsurface core with mean ASV of ∼−0.45 m s^{-1} centered at ∼180 m (Figure 3b). The 1996 moored record by *Molcard et al.* [2001] also suggested the presence of the deep flow maximum. The surface core shows the highest variability. The two-core structure to the ITF in Ombai Strait is also evident in the mean geostrophic flow across the repeat XBT line PX22, which crosses the inflow of Ombai Strait just north of Alor Strait between Alor and Wetar islands [*Wijffels et al.*, 2008].

[19] In Timor Passage, the ITF is strongly surface trapped in the upper ~200 m. Interestingly even the surface flow is strongest over the deep sill itself (Figure 3c) while there is more variability in the flow to the north near Roti, as also suggested by Figure 2c. There is a secondary weak core of Timor ITF centered ~1200 m, also found in earlier mooring observations [*Molcard et al.*, 1996]. This deeper core is associated with the Indonesian Intermediate Water (IIW) carried by the ITF [*Talley and Sprintall*, 2005]. Below ~1600 m on the sill, the mean ASV is directed toward the Timor basin, although there is high variability associated with this flow (Figure 3c). Overall though, Timor exhibits much weaker upper ocean velocity variability than Lombok or Ombai Straits, which likely reflects its topographical isolation from the active equatorial Indian and Nusa Tenggara coastal waveguides.

[20] In the following, we show transports calculated using a constant surface shear model for all straits, and our w-block lateral interpolation for Ombai and Lombok and a cubic lateral interpolation for Timor. These schemes are considered our most likely or ''best'' interpolation schemes. However, collectively the schemes described earlier give us a range of possible values for transport. Estimates resulting from the various cross-passage schemes are most sensitive in Ombai Strait, because of the totally different characteristics of the flow in the north and south (Figure 3b), and in Timor Passage, because of the width of the strait and the large shallow shelf region south of Timor Ashmore where we have no measurements (Figure 3c). Similarly, the choice of the surface layer model (3) would be a lower bound on the transport estimates. The range of transport from the combination of cross-passage and surface layer schemes will be reported as our uncertainty error. Other errors may be introduced by measurement error, but this contribution is likely much smaller compared to our assumptions about the flow structure across the passage or at depths where direct instrument measurements are missing.

3. Transport Variability

[21] Winds from the Pacific and Indian Oceans and over the regional Indonesian seas modulate the ITF on a wide variety of timescales via the excitation and propagation of planetary waves [*Clarke and Liu*, 1994; *Meyers*, 1996; *Sprintall et al.*, 2000; *Potemra*, 2001; *Wijffels and Meyers*, 2004; *McClean et al.*, 2005]. Because of its proximity to Asia and Australia, the circulation and transport within the Indonesian seas has a large seasonal variation due to the influence of the reversing annual wind patterns associated with the Asian-Australian monsoon system [*Clarke and Liu*, 1993; *Masumoto and Yamagata*, 1996]. Relatively dry winds blow from the southeast across the region during June–August, referred to as the Southeast Monsoon (SEM). Moist warm air blows from the west during the Northwest Monsoon (NWM). Between these times, the intertropical convergence zone passes across the equator in both the Pacific and the Indian Oceans, and embedded in this are westerly wind bursts that mark the Monsoon Transition Seasons (MTS). Transport is expected to be maximum during the SEM when the winds drive strong Ekman divergence from the internal seas [*Wyrtki*, 1987; *Gordon and Susanto*, 2001]. On interannual timescales, most models and observations point to a weaker ITF during El Niño in response to the Pacific trade-wind reversals that subsequently lowers western Pacific sealevel [*Wyrtki*, 1987; *Clarke and Liu*, 1994; *Meyers*, 1996; *Gordon et al.*, 1999; *Wijffels and Meyers*, 2004; *McClean et al.*, 2005; *England and Huang*, 2005]. Less is known about the role of the Indian Ocean Dipole (IOD) on ITF transport variability, and its associated modulation of local and remote equatorial Indian Ocean winds [*Saji et al.*, 1999]. A shallow pressure gauge array (SPGA) with surface temperature and salinity measurements deployed within the exit passages from 1995 to 1999 revealed a complex and different interannual transport response in each passage [*Hautala et al.*, 2001; *Sprintall et al.*, 2003]. However, that deployment period included both the major 1997–1998 El Niño and IOD events that were in phase that year. In addition, models [e.g., *Potemra et al.*, 2003] and the long-term XBT observations [*Wijffels and Meyers*, 2004] suggest that the low frequency signal from both the Indian and the Pacific Ocean is probably stronger in the deeper layers, and so not easily detected by the surface measurements during the SPGA deployment period.

[22] In this section we examine the distribution of transport with depth and its subinertial variability (section 3.1) at seasonal (section 3.2) and interannual timescales (section 3.3). The seasonal cycle is based on the annual and semiannual harmonics from the 3-year INSTANT time series, and ''interannual'' anomalies are then formed by a 75-day low pass of the seasonal anomalies. The mean transport profile for each exit passage and the associated heat flux are discussed in section 3.4. In section 3.5, the transport per unit depth time series are integrated to various depth levels to produce the total transport time series and its seasonal variability. Finally, in section 3.6 we present the 3-year mean INSTANT total transports for each of the three passages.

3.1. Vertical Distribution of the Subinertial Flow

[23] The INSTANT observations reveal a highly baroclinic and complex flow featuring strong phase changes with depth. After the tidal band, intraseasonal variability dominates the flow. Strong similarities are found in the 3-year time series of transport per unit depth over the upper 300 m in both Lombok (Figure 4a) and Ombai Straits (Figure 4b). The surface ITF is typically strongest during the SEM from July through October, while the NWM from December through March is punctuated by shallow transport reversals (i.e., away from the Indian Ocean) in both straits. Reversals during this monsoon phase have a clear intraseasonal variability and given the relatively shallow vertical penetration, they are most likely a locally wind-driven Ekman dynamical response (Wijffels et al., in preparation). When these surface reversals occur, the main ITF is found in the subsurface. During the NWM, the Ombai Strait ITF transport can extend to almost 1200 m depth, and is just as strong as that found at the surface during the SEM.

[24] The strong flow reversal in May 2004 from the surface to 300 m in Lombok Strait (Figure 4a) and to ~700 m in Ombai Strait (Figure 4b) is the clear signature of a downwelling Kelvin wave generated in response to wind reversals in the equatorial Indian Ocean during this MTS [*Clarke and Liu*, 1994; *Sprintall et al.*, 2000; *Molcard*

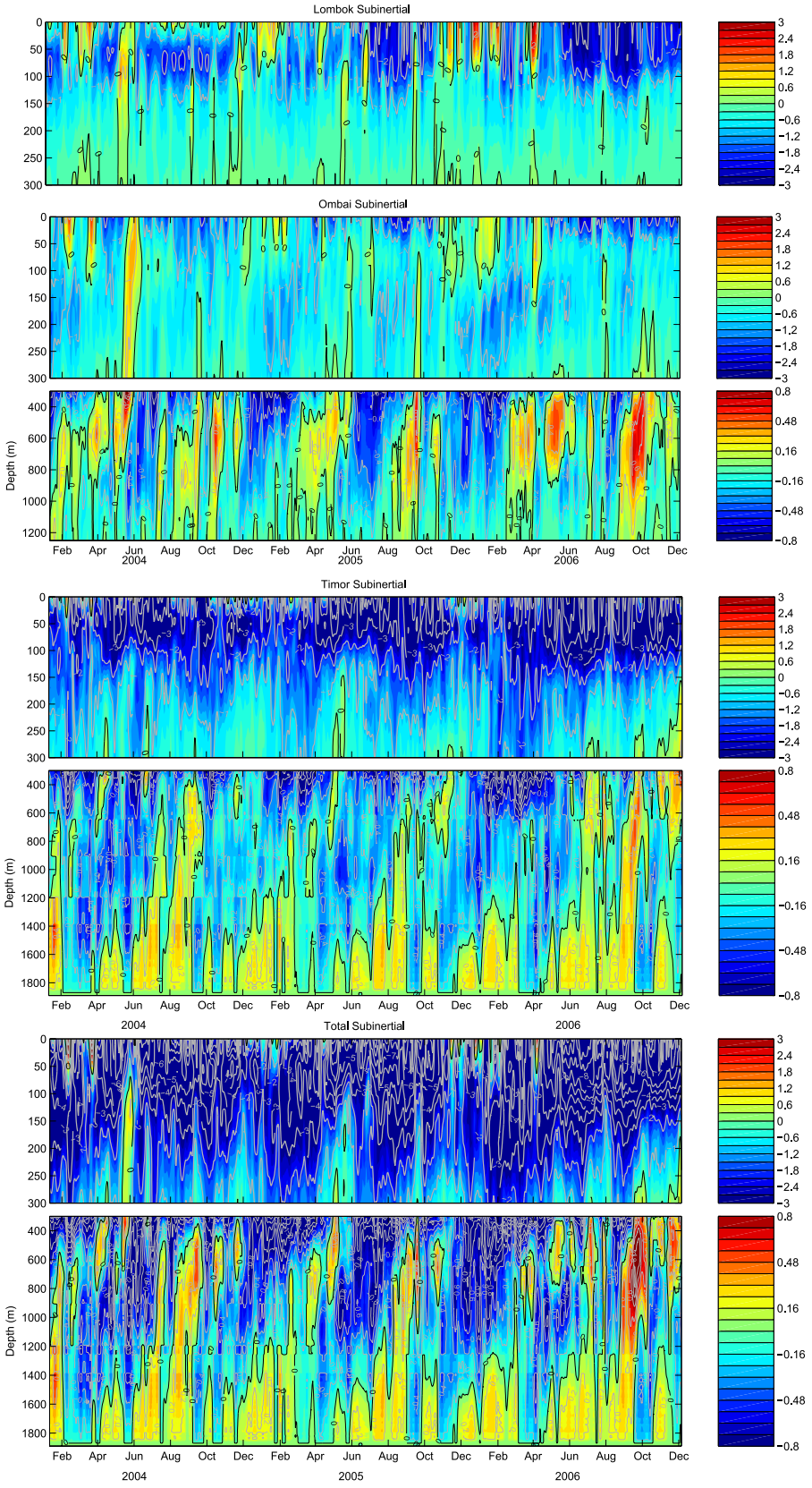

Figure 4. Vertical distribution of subinertial transport per unit depth (10^{-2} Sv m^{-1}) for (a) Lombok Strait, (b) Ombai Strait, (c) Timor Passage, and (d) the total transport to the respective sill depths. Note change of vertical and transport scales for depths of >300 m.

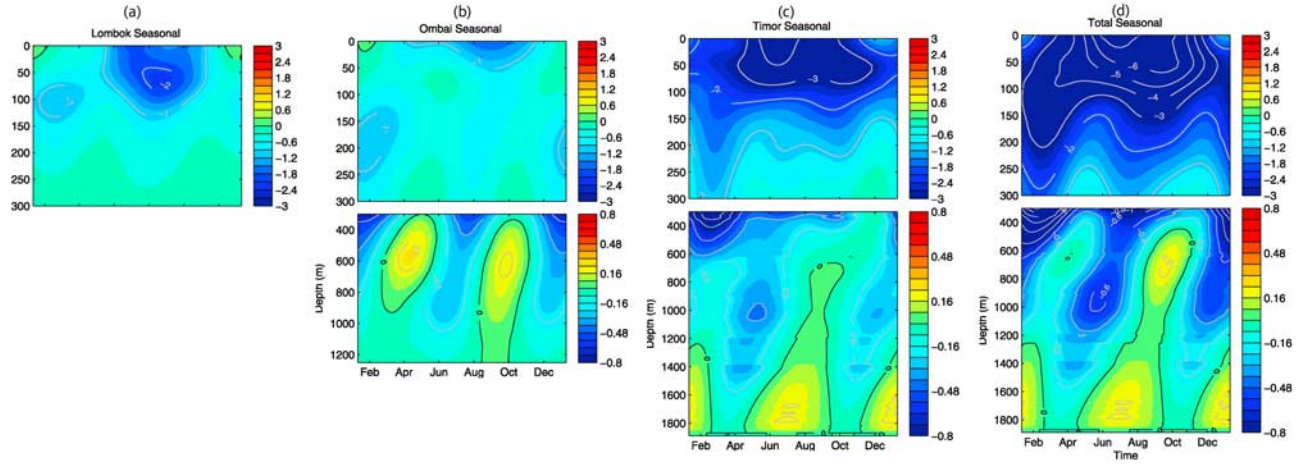

Figure 5. Seasonal cycle of transport per unit depth (10^{-2} Sv m^{-1}) for (a) Lombok Strait, (b) Ombai Strait, (c) Timor Passage, and (d) the total transport to the respective sill depths. Note change of vertical and transport scale for depths of >300 m.

et al., 2001]. The surface layer reversals with deep reaching precursors seen in both these straits during the MTS periods of April 2005, late June 2005 and April 2006 are also likely related to Kelvin wave events. Occasionally the MTS Kelvin wave reversals in both straits are only found at depth and have no significant surface signature (e.g., September 2004, May 2005, September 2005).

[25] There is little in common between the 0 and 300 m variability in Timor Passage and that found in Lombok and Ombai Straits (Figure 4). Timor features weaker variability on the intraseasonal timescale, with flow reversals rare above 300 m. At subthermocline to intermediate depths, flow reversals in Timor Passage are also evident during the MTS (Figure 4c), but with stronger events occurring in the second annual MTS (~September) compared to Ombai where reversals are strong during both MTS (Figure 4b). Reversals in Timor become more prevalent from July 2006 through the end of the time series (Figure 4c). Below 1400 m in Timor Passage, relatively strong intraseasonal reversals are found over the sill, and it is thought these may be related to Kelvin wave excitation in the equatorial Indian Ocean on this timescale.

[26] The strong surface flow in Timor dominates the total subinertial transport, although the shallow NWM reversals in Lombok and Ombai are also evident (Figure 4d). In the upper 300 m, the May 2004 Kelvin wave reversal stands out as an extraordinarily strong event compared to the other MTS reversals over this depth range (Figure 4d). Below 300 m, the semiannual reversals in Timor and Ombai punctuate the strong deep ITF total transport record, and the September 2006 reversal from ~250 m to the bottom is the strongest anomaly over this depth range.

3.2. Seasonal Transport per Unit Depth

[27] In all three straits the surface to thermocline flow is toward the Indian Ocean during most of the year, except during the NWM when the upper ~20 m weakly reverses in Ombai (Figure 5b) and Lombok (Figure 5a) Straits, and relaxes in Timor Passage (Figure 5c). Thus during the NWM the main core of the ITF is subsurface and about -1.0 to -1.5×10^{-2} Sv m^{-1}, extending from 60 to 150 m in Lombok and from 100 to 600 m in Ombai. During the SEM, surface transports are a maximum in June–July in Lombok (Figure 5a) and Timor (Figure 5c), while 50–80 m transports reach a maximum in August in these straits when Ombai surface transport is maximum (Figure 5b). Thus above 150 m, the total ITF displays a complex vertical phasing in the seasonal cycle, with the surface and 100 m transport being out of phase (Figure 5d). This rapid phase shift is similar to that found in the annual Rossby wave measured at the Arafura shelf break [*Wijffels and Meyers*, 2004] and likely reflects the control of this wave on the pressure field, particularly at the southern slope of Timor Passage.

[28] At depths below the thermocline, semiannual variability dominates all straits, although again the phasing of this signal differs slightly from strait to strait. Strong reversals of $\sim 0.25 \times 10^{-2}$ Sv m^{-1} are evident in Ombai Strait during the MTS (Figure 5b). The clear upward phase propagation is the signature of downward energy propagation by a free coastal Kelvin wave. In April–May the reversed flow extends from 400 to 800 m and in September–October from 400 to 1000 m. Interestingly, the phase propagation is slightly different during the two reversals. Furthermore, the maximum depths of these signatures closely correspond to the sills both north (~900 m) and south (~1150 m) of Sumba Island on the western edge of the Savu Sea (Figure 1). The different upward phase breaks in Ombai Strait may indicate that during each MTS, the Kelvin waves are following different pathways north and south of Sumba Island and into the Savu Sea. In Timor Passage a strong semiannual reversal of $\sim 0.25 \times 10^{-2}$ Sv m^{-1} with upward phase propagation is evident from the 1890 m sill up to ~700 m (Figure 5c) during July–August and again in December–January. Clearly some of the Kelvin wave energy driving reversals in Lombok Strait is siphoned off and continues along the Nusa Tenggara waveguide to Ombai, and further, some of the energy is trapped below the controlling sill depths for the Savu Sea causing the deep reversals in Timor Strait. Thus when combined, the total transport (Figure 5d) shows the dominance of the semiannual wave, with a fairly constant upward phase propagation from the bottom to 150 m depth, where

the top part of the wave (150–700 m) is found in Ombai (Figure 5b) and the bottom part of the wave in Timor (Figure 5c). The semiannual energy dominating both the deep Ombai and Timor flows, results in peaks of the export of IIW transport of $\sim -0.5 \times 10^{-2}$ Sv m^{-1} during the MTS (Figure 5d).

3.3. Interannual Transport per Unit Depth Anomalies

[29] The 3-year INSTANT deployment period coincided with a relatively neutral or very weak warm phase of ENSO from the initial deployment in January 2004 until ~September–October 2005, followed by a brief weak cool phase until April 2006, with stronger El Niño conditions developing until the mooring recovery in December 2006. The developing El Niño conditions in the Pacific during this latter period also coincided with a strong IOD positive phase in the Indian Ocean that terminated in December 2006–January 2007 [*Vinayachandran et al.*, 2007; *Horii et al.*, 2008]. These conditions are reflected in the zonal equatorial wind stress anomalies for the Pacific and Indian Oceans (Figure 6a): Pacific wind changes are weak compared to those in the Indian Ocean during the INSTANT period.

[30] Unexpectedly we find interannual transport anomalies in all three straits to be very similar in the upper 150 m (Figures 6b–6d): a relatively strong reversal in 2004, near mean in 2005 except for two relaxations (June and December 2005), and then a steady strengthening in all passages after December 2005. Below 150 m, flow in Lombok is generally weak, while that in Ombai and Timor are slightly out of phase (Timor lags by ~1–2 months) until after May 2006 when the deep ITF reverses in both passages and the surface ITF strengthens. This clear synchronization of all passages at all depths coincides with the advent of the strong Indian Ocean wind changes associated with the IOD positive phase (Figure 6a). It is likely that the reversals in the lower layer are related to the prolonged easterly wind anomalies that occur in the tropical Indian Ocean during IOD events, that are known to force upwelling Kelvin waves [*Yu and Rienecker*, 1999; *Horii et al.*, 2008] that impact the flow and properties along the coastal waveguide [*Sprintall et al.*, 1999, 2003]. Of note, the anomalously strong surface ITF (-2 to -3×10^{-2} Sv m^{-1}) during this latter part of the record (Figure 6e), which occurred during the concurrent 2006 IOD and El Niño events, is opposite to that found during the weaker El Niño over the first 18 month INSTANT deployment period, when the surface flow was much weaker than normal (2 to 3×10^{-2} Sv m^{-1}).

3.4. Mean Transport Profile and Heat Fluxes

[31] In both Timor and Lombok Straits, transports are primarily surface intensified, although both straits have a weak subsurface maximum at 50–60 m (Figure 7). The Ombai Strait transport profile features both a surface maximum and an equally strong subsurface maximum near ~180 m depth (Figure 7). Timor Passage has a slight subsurface maximum at ~1000 m transporting the core of IIW. Above 1500 m, the total Throughflow transport is all toward the Indian Ocean and similar in structure to the Timor transport profile. Below 1500 m, the Timor mean transport profile reverses with inflow of about 0.15 Sv flows into the Timor Trough that then exits back into the Indian Ocean below ~1300 m (noting that the upstream sill into the Banda Sea is around 1250 m).

[32] Due to fishing and shipping pressures, during INSTANT the temperature measurements were only taken to within 100 m of the surface. Thus to estimate the heat transport of the flows, we use a mean seasonal cycle of temperature from a high resolution temperature climatology produced for the region based on quality-controlled historical data [*Gronell and Wijffels*, 2008] using the topography-following mapping method by *Dunn and Ridgway* [2002]. Over comparable depth ranges, the available temperature profiles from the moorings agreed very well with the climatological values, with vertical temperature changes being much larger than variability on any given pressure level. Heat fluxes are presented as the effective temperature of the total throughflow, that is, the transport-weighted temperature (TWT).

[33] It is the vertical distribution of transport through each strait that, to a large extent, sets the heat flux carried by the ITF flow, and thus the TWT (Figure 8). Due to its shallow sill, Lombok carries the warmest ITF (21.5°C), Timor the next warmest (17.8°C) because it is also surface-intensified, and Ombai the coldest (15.2°C) because of the maximum ITF at depth (Figures 7 and 8). The TWTs in Lombok are warmest during the time of strongest transport in SEM when the flow is surface intensified, and coldest during the NWM when the surface reversals reduce the heat transport by sending the warmest waters against the mean ITF (Figure 8). Ombai TWT is highly variable, and reflects the strongly variable and deep-reaching shear in that strait: warmest TWT occurs when the cold deep flow is opposed to a warm thermocline ITF, and coldest TWT occurs when the deep flow augments the ITF. Hence Ombai TWTs show a strong and distinct semiannual signal associated with the dominant semiannual transport variability at depth (Figure 5b). As both the shear and transport in Timor Passage is less variable than in Ombai, the TWT here are steadier although semiannual variability is also evident (Figure 8). From May 2006 onward, the TWT in all straits rises, reflecting the surface intensification of the ITF associated with the IOD wind-forcing (Figure 6).

3.5. Total Transport Variability

[34] The time series of total transport in the upper 300 m shows great similarity in Lombok and Ombai Straits, and is characterized by many intraseasonal reversals (Figure 9a), underscoring the dominance of the intraseasonal variability over the seasonal and interannual. There is a phase lag of ~4–5 days between the peak reversals from Lombok to Ombai, which is commensurate with the speed of the first mode baroclinic Kelvin wave along the Nusa Tenggara waveguide. However, the surface layer transport also responds to local wind effects (Wijffels et al., in preparation), and it may be that the phase lag is simply an artifact of the timing of the wind events in each passage. Both straits also show a semiannual signal in 0–300 m seasonal transport variability although it is slightly stronger in Ombai (thin lines in Figure 9 and Table 3). Ombai Strait has roughly equal amplitude total ITF transport maxima of -4 Sv in August and February and minima of -2.2 Sv in May and -2.6 Sv in November (Figure 9a, Table 3). Compared to Ombai, Lombok Strait has a weaker maximum

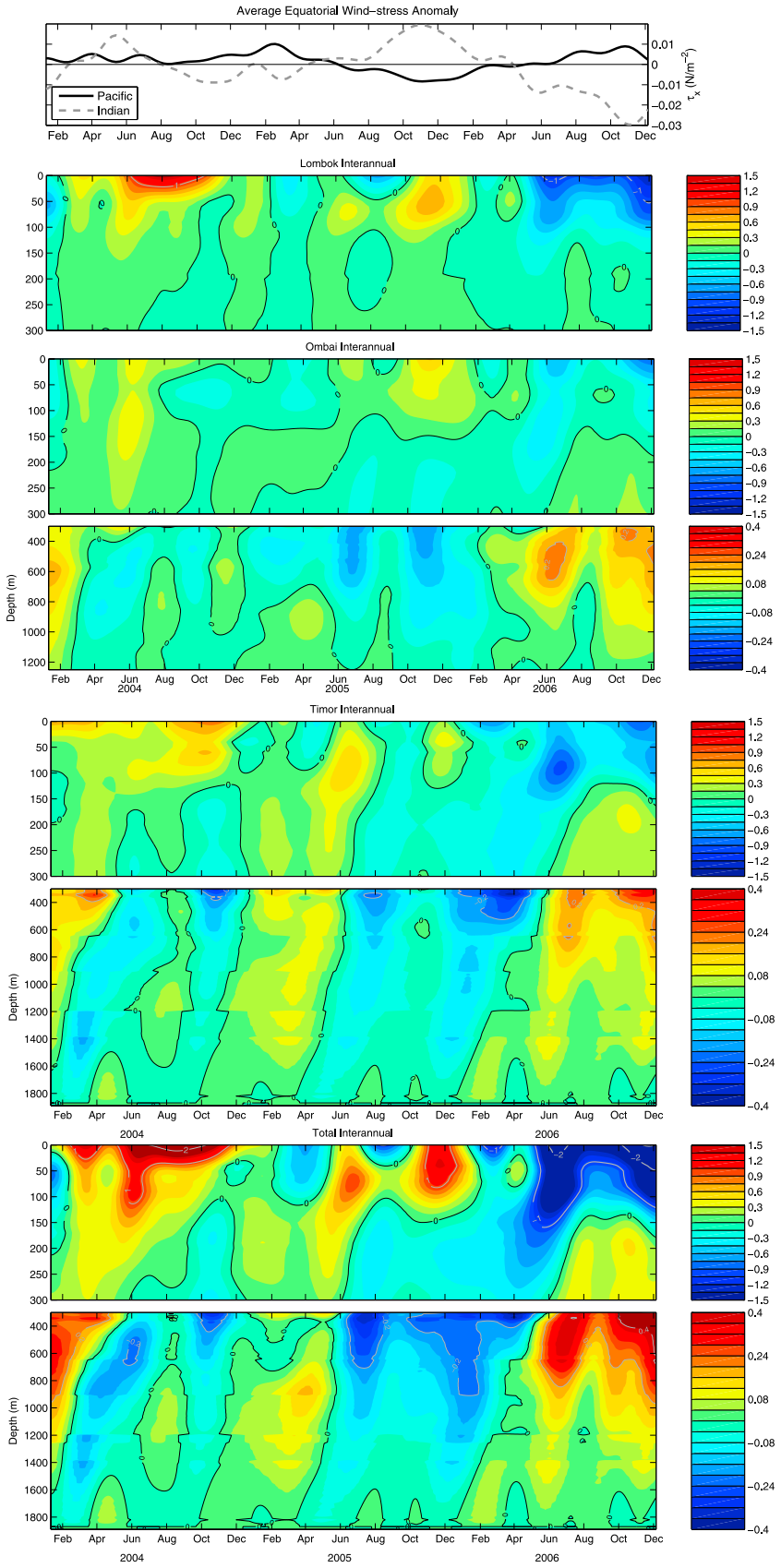

Figure 6. (a) Average wind anomalies along the equator (N m^{-2}) for the Indian (dashed) and Pacific Ocean (solid). Time series of interannual transport per unit depth anomalies (10^{-2} Sv m^{-1}) for (b) Lombok Strait, (c) Ombai Strait, and (d) Timor Passage, and (e) the total transport to the respective sill depths. Note change of vertical and transport scale for depths of >300 m.

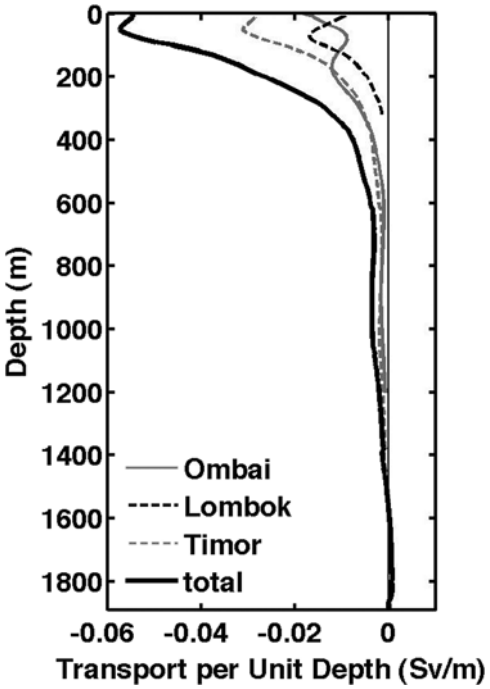

Figure 7. Mean transport profile (Sv m^{-1}) for Lombok Strait (black dashed), Ombai Strait (gray solid), Timor Passage (gray dashed), and total of the three passages (black solid).

of −2.2 Sv in February and a smaller minimum of −1.39 Sv in November (Table 3). The time series of total transport in the upper 300 m in Timor Passage is relatively steadier and larger compared to Lombok and Ombai Straits and while there are relaxations, there are no reversals (Figure 9a). The annual cycle clearly dominates the upper-layer transport in Timor Passage (Figure 9a), with a minimum of −4 Sv in December and maximum of −5.8 Sv from around April right through September (Table 3).

[35] Below the Lombok sill (300m), transports between 300 and 600m (Figure 9b) show a regular semiannual transport cycle in Ombai, but a much more variable cycle in Timor Passage, sometimes nearly in phase with Ombai (e.g., 2005) but out of phase at other times (2004). In early 2006, Timor ITF peaks strongly while Ombai is weakening. Deeper, between 600 and 1200 m (Figure 9c), Ombai and Timor both show a strong semiannual variability, which is only weakly lagged. Thus the total ITF variability is very strongly semiannual at 600–1200 m depths, due to the near phase-locking of both these deep straits, giving an enhanced export of IIW during January–February and July–August. Toward the end of 2006 the net IIW actually weakens and reverses, indicating an import of intermediate waters into the internal seas.

[36] The full depth transports show that while Ombai carries significant transport toward the Indian Ocean below 300 m, most of the ITF enters the Indian Ocean through Timor Passage (Figure 9d). Furthermore, the total seasonal cycle in transport is clearly out of phase between Ombai and Timor (Table 3), and our discussion above indicates that this mostly occurs above 600 m. When the ITF transport is strong in Ombai Strait in July–August (−6.6 Sv) and December–January (−7.9 Sv), Timor transport is reduced (Figure 9d). Transport through Ombai Strait is minimum during the monsoon transition periods of April (−2.5 Sv) and September (−2.7 Sv) when the downwelling Kelvin waves associated with the Wyrtki Jets [*Wyrtki*, 1973] reverse the transport at depth (Figure 4b). In particular, during the April–May period, transport through Timor Passage is strongest (−9 Sv) suggesting that the Wyrtki Jets may play a major role in controlling the gating of the flow above ~600 m through the exit passages on annual timescales. Finally, although Timor Passage carries most of the transport, the intraseasonal variability in transport is greater in Ombai and Lombok and is in phase, thus dominating the variability of the total ITF transport summed through all three passages (Figure 9d).

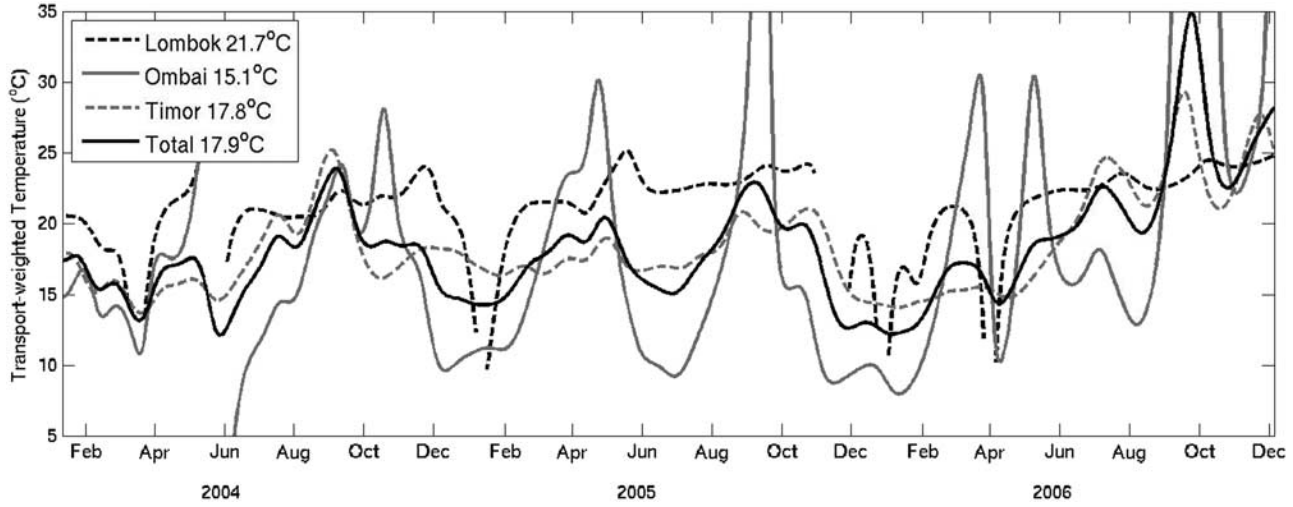

Figure 8. Time series of transport weighted temperatures (TWT, °C) for the Lombok Strait (black dashed), Ombai Strait (gray solid), Timor Passage (gray dashed), and the total ITF (black solid). Mass and heat transports were low-passed by 45 days before calculating the TWT. Mean TWTs are indicated in the legend.

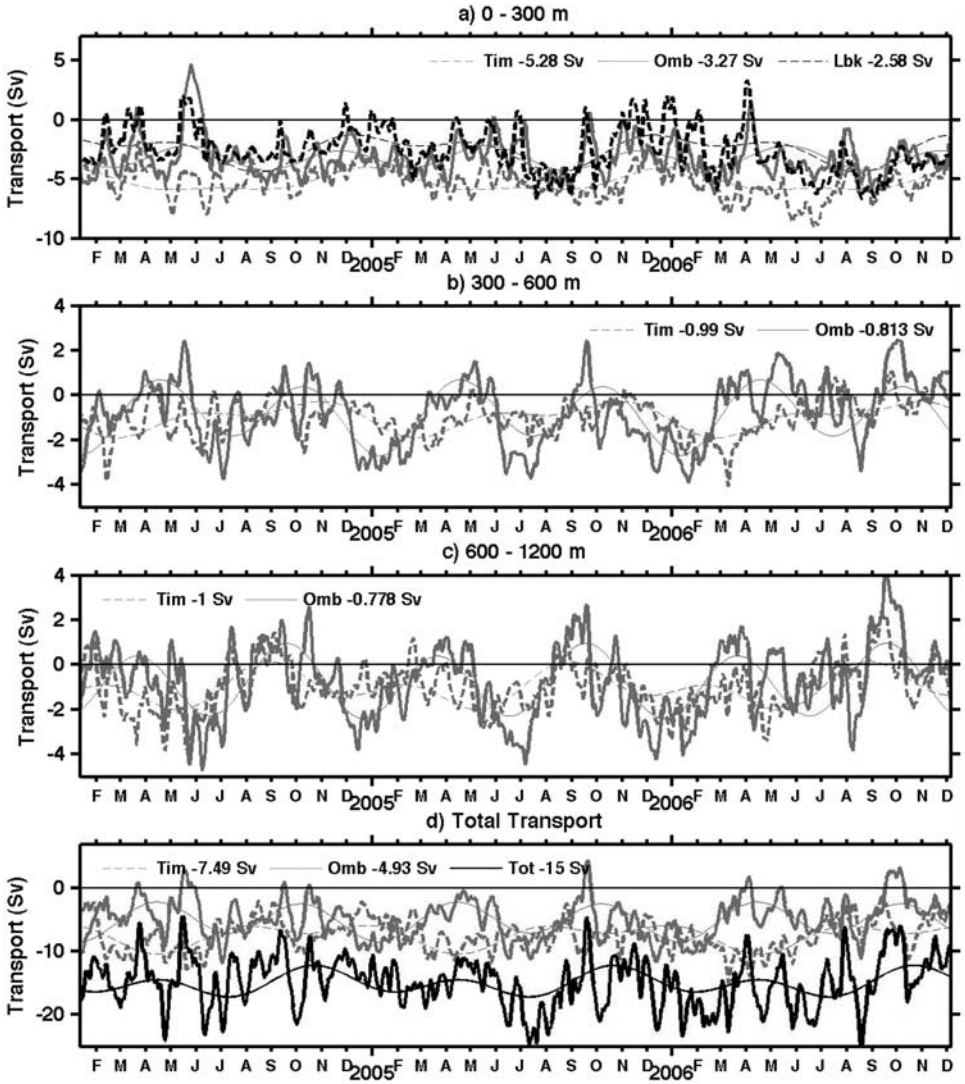

Figure 9. Time-series of transport (Sv) for Lombok Strait (black dashed), Ombai Strait (gray solid), and Timor Passage (gray dashed) for the depth interval (a) 0–300 m, (b) 300–600 m, (c) 600–1200 m, and (d) 0–1200 m. The total transport (black) is shown in Figure 9d. Note the change in transport scales. Mean transports over each depth range are indicated in the legend.

3.6. Total Mean Transports

[37] Over the 3-year INSTANT period (January 2004–December 2006) the total ITF transport from the surface to respective sill depths of the three exit passages was −15.0 Sv (i.e., toward the Indian Ocean), ranging from −10.7 Sv to −18.7 Sv (Table 1). Of this total transport half, −7.5 Sv (range: −6.2 Sv to −10.5 Sv), entered the Indian Ocean through Timor Passage (0–1890 m), with −4.9 Sv (range: −2.7 Sv to −5.0 Sv) entering through Ombai Strait (0–1200 m), and −2.6 Sv (range: −1.8 Sv to −3.2 Sv) through Lombok Strait (0–300 m). Over two thirds (11.2 Sv) of the total transport occurred in the upper 300 m, again,

Table 3. Monthly Transport (Sv) Estimates in Lombok, Ombai, and Timor Straits[a]

Passage and Depth Range	January	February	March	April	May	June	July	August	September	October	November	December
Lombok (0–300m)	−1.90	−2.19	−2.08	−1.91	−2.26	−3.19	−4.13	−4.29	−3.46	−2.20	−1.39	−1.41
Ombai (0–300m)	−3.76	−3.95	−3.39	−2.54	−2.23	−2.81	−3.76	−4.22	−3.80	−3.00	−2.64	−3.06
Timor (0–300m)	−4.33	−4.98	−5.59	−5.86	−5.83	−5.75	−5.80	−5.84	−5.59	−4.99	−4.32	−4.03
Ombai (0–1200m)	−7.84	−5.40	−2.88	−2.46	−4.41	−6.57	−6.67	−4.63	−2.73	−3.12	−5.65	−7.99
Timor (0–1890m)	−7.06	−7.99	−8.80	−9.07	−8.66	−7.85	−7.07	−6.57	−6.32	−6.18	−6.13	−6.37
Total ITF	−16.8	−15.6	−13.8	−13.4	−15.3	−17.6	−17.9	−15.5	−12.5	−11.5	−13.8	−15.8

[a]For the 0–300 m depth range; 0–1200 in Ombai Strait; 0–1890 m in Timor Passage; and for the combined total Throughflow transport (Lombok 0–300 m, Ombai 0–1200 m, Timor 0–1890 m).

mostly through Timor Passage (−5.3 Sv), with −3.3 Sv leaving through Ombai Strait and −2.6 Sv through Lombok Strait.

4. Discussion and Conclusions

[38] The INSTANT field program, consisting of a three-year deployment of 11 moorings in the major inflow and outflow passages of the ITF, provides an unprecedented data set revealing how this complex and fascinating region responds to local and remote forcing and at many timescales never before well-resolved. For the first time, simultaneous multipassage direct observations of *in situ* velocity of the ITF clearly reveal the gating of the flow between the three major outflow channels in response to the monsoon cycle and gives insight into changes due to the ENSO and IOD climate modes. The focus of this paper is the transport variability and heat fluxes through the three major outflow passages (Lombok Strait, Ombai Strait, and Timor Passage) which collectively convey the total ITF transport profile and the associated heat flux into the southeast Indian Ocean.

[39] In this section we provide details of the major new results of the ITF mean flow and variability that were revealed by the INSTANT measurements in the exit passages. However, for the researcher interested in knowing the bottom-line estimates of ITF transport through each of the exit passages we refer them to the seasonal transport estimates in Table 3, and section 4.6 where we present our best total ITF transport of −15.0 Sv into the Indian Ocean.

4.1. Dominant Monsoon Wind Forcing

[40] Transport time series in the surface layer of the three passages are very complex, due to the effects of local winds as well as the remote large-scale forcing. To first order, the surface to thermocline seasonal cycle is dominated by the regional monsoon forcing. During the NWM, the shallow transport is reversed in Lombok and Ombai due to episodic locally wind-driven Ekman currents (Wijffels et al., in preparation) and reduced in Timor, which drives the core ITF deeper. During the SEM, divergence from the Banda Sea [*Wyrtki*, 1987; *Gordon and Susanto*, 2001] combined with the lower sea level off the south coast of Nusa Tenggara [*Wyrtki*, 1987], draws waters into the Indian Ocean and surface transport in Lombok and Ombai is maximum. In Timor Passage the ITF is largely surface-intensified, and also relatively strong and steady during this monsoon period.

[41] The dynamics of what limits and partitions the transport through the three straits during times of strong ITF flow is not well understood. Clearly local wind-driven divergence in the Banda Sea modulates the seasonal cycle and must affect the along-strait pressure gradients driving the flow [*Wyrtki*, 1987]. However, remote winds from intraseasonal [*Sprintall et al.*, 1999] through to interannual periods [*Wijffels and Meyers*, 2004], drives wave energy that also radiates into the region and affects the currents. Both Ombai and Timor show the signatures of free semi-annual Kelvin waves (upward phase propagation), but they are evident over different depth ranges: 150–1250 m in Ombai, and 700–1890 m in Timor. Above these depths the seasonal cycle is more complex in both straits. We suspect that three influences are at work: the remotely driven Indian Ocean Kelvin waves; local wind stress changes; and possibly Banda Sea wind stress changes that may excite coastally trapped waves in the Arafura/Timor waveguides as well as Rossby waves that radiate out across the Banda Sea. Model experiments are required to help diagnose the controlling forces.

4.2. Evidence of Remotely Driven Kelvin Waves in All Exit Passages

[42] The INSTANT and historical data show overwhelming evidence for the presence of Kelvin waves in both Lombok Strait and Makassar Strait [*Sprintall et al.*, 2000; *Wijffels and Meyers*, 2004; *Gordon et al.*, 2008], supporting those theoretical models that had suggested Indian Ocean forced Kelvin wave energy can indeed penetrate into the internal Indonesian seas [*Durland and Qiu*, 2003; *Johnson and Garrett*, 2006]. Transport reversals are also apparent in Ombai Strait further east along the Nusa Tenggara coastal waveguide, corroborating earlier evidence that an Indian Ocean Kelvin wave can penetrate through the Savu Sea and beyond [*Hautala et al.*, 2001; *Molcard et al.*, 2001]. An upward vertical phase tilt is evident in both the transport (Figures 5 and 6) and temperature (not shown) data of these straits, which is consistent with the downward propagation of energy in Kelvin waves as they pass along the Nusa Tenggara coastal waveguide. Clearly, some of the Kelvin waves drive strong surface transport reversals in both Lombok and Ombai Straits, while at other times, as also found in Timor, the deep reversals do not have strong surface signatures (Figure 4). In the southern hemisphere, free Kelvin waves disperse along raypaths both vertically and horizontally such that the coastline is on the left in the direction of the wave propagation [*McCreary*, 1984]. Both timing and location of the wind-forcing are important for the dispersion: higher-frequency and/or remotely generated waves dive more steeply than low-frequency or locally generated waves. Commensurate with this vertical ray-tracing theory, Kelvin waves excited from semiannual to intraseasonal timescales along the equator in the Indian Ocean, dive with distance along the waveguide along respectively deepening raypaths [*Wijffels and Meyers*, 2004]. Thus a remotely forced Kelvin wave packet could have dived sufficiently that, by the time it encounters Lombok, much of its energy is below the sill depth (300 m) and can thus proceed across the deeper Savu Sea sills to drive reversals in Ombai Strait without losing much of its energy via transmission through Lombok. Similarly, the steeper diving, higher-frequency intraseasonal energy can bypass the Savu Sea sills to directly cause the deeper reversals observed in Timor. Interestingly, the deeper reaching Kelvin wave during the second MTS in Ombai that may come from across the Savu/Dao Straits, also coincides with when the semiannual signal is stronger in Timor Passage (Figure 5). What proportion of the Kelvin wave energy is transmitted through Lombok Strait versus that passing across the strait and remaining in the coastal waveguide to reach Ombai Strait (both north and south of Sumba Island) and Timor Strait are the subject of future analysis.

[43] Perhaps one of the most important implications from the INSTANT observations of the passage of the Kelvin waves and the SJC system through Ombai Strait is that this

delivers Indian Ocean water into the internal Banda Sea where the relatively isohaline Indonesian Throughflow Water (ITW) is formed. This suggests that, along with input sources originating from the North and South Pacific, the saltier Indian Ocean water carried by the SJUC [*Atmadipoera et al.*, 2009] can also potentially participate in the formation of ITW. Historically, most water mass analysis studies [e.g., *Ffield and Gordon*, 1992; *Hautala et al.*, 2001] have ignored the Indian Ocean source. Our study suggests its contribution should be carefully considered in future comprehensive studies of the formation of ITW. The influence of the saltier water carried by the Kelvin waves, along with tidal mixing, air-sea heat, freshwater and momentum forcing in the internal seas, also play a likely role in setting the stratification of the ITW within each exit passage. Unfortunately, because of the missing property measurements in the upper 100 m at the INSTANT moorings, we are unable at present to adequately resolve the vertical stratification within each exit passage. Ongoing analysis will investigate the use of the high-resolution temperature climatology [*Gronell and Wijffels*, 2008] used in the TWT calculation, combined with the INSTANT measurements at depth, for this purpose.

4.3. Variability of the Indonesian Intermediate Water

[44] INSTANT provides the first simultaneously observed time series of the IIW component of the ITF in Ombai Strait and Timor Passage. Distinct strong cores of IIW are present at 800–1200 m depth in Timor Passage with weaker cores present in Ombai Strait from 600 to 1000 m depth. The IIW has a strong semiannual signal (Figure 9c) with maxima occurring in the MTS. Total IIW during the INSTANT period was −1.8 Sv, with −1 Sv exiting Timor Passage and −0.8 Sv exiting Ombai Strait. For the Ombai Strait IIW to enter the Indian Ocean and the SEC, it must exit the Savu Sea through the deeper Savu/Dao Straits (∼1150 m) south of Sumba Island (Figure 1). Unfortunately there are no direct measurements of the flow in this passage over this depth range, as the deeper current meters deployed by *Molcard et al.* [1994] during a 1989–1990 mooring deployment just west of Dao Strait were lost. However, salinity and silica profiles show strong evidence of IIW just to the west of Savu/Dao Strait and Timor Passage [*Fieux et al.*, 1994, 1996; *Wijffels et al.*, 2002; *Talley and Sprintall*, 2005]. IIW transports derived from the JADE [*Fieux et al.*, 1994, 1996] synoptic hydrographic surveys were −2.9 Sv in August 1989 and −3.0 Sv during February 1992 [*Talley and Sprintall*, 2005], which are in agreement with that found in INSTANT during these months (Figure 9c).

4.4. ITF Response to the 2006 Indian Ocean Dipole

[45] Despite the differences and complexities in the phasing of the seasonal variability, the interannual anomalies in all three passages show remarkable similarities, particularly in response to the strong positive IOD during the last year of the INSTANT deployment period. The transport variability during both the ENSO and IOD phases over the 3-year period show a clear phase break occurring at ∼150 m depth with the upper layer and lower layer frequently opposed to each other. Using numerical model output, *Potemra et al.* [2003] demonstrated a complex relationship between the gating of the transport through the outflow passages, with the interannual forcing from the Pacific and Indian Oceans acting independently on the different vertical layers of the ITF, and thus not having a clear signal in the total depth-integrated transport. The total ITF during the INSTANT time period plainly shows this to be the case: the enhanced surface transport is largely canceled by the transport reversals at depth in the total transport time series (Figure 9d). *Masumoto* [2002] showed a much stronger correlation of ITF upper layer transport with a mode of surface dynamic height related to interannual wind variability in the Indian Ocean than that associated with ENSO. The correlation was such that there was increased warm water divergence of the upper 230 m layer out of the Indonesian seas during IOD periods [*Masumoto*, 2002]. During INSTANT, transport in the surface layer during the 2006 IOD is strongly toward the Indian Ocean and reversed below, driving up the heat transport of the ITF (Figure 8).

[46] In Makassar Strait, previous observations suggested greater transport and deeper thermocline during La Niña, with the opposite occurring during the El Niño phase [*Gordon et al.*, 1999; *Ffield et al.*, 2000]. This response was also found during the INSTANT observational period in Makassar Strait [*Gordon et al.*, 2008]. In the outflow passages, the relaxation of the upper 150 m during the 2004 weak El Niño event agrees with that found in Makassar (both historically and during INSTANT), while during the 2006 El Niño that coincides with the IOD event, the ITF is stronger in the outflow passages over this depth range. Total ITF transport was −13.8 Sv in 2004 and −15.4 Sv in 2006. With such a short record, it may be difficult to separate the competing remote influences from ENSO and the IOD on the ITF transport variability during 2006.

[47] The relationship of the ITF transport variability to the remote wind-forcing from the Indian and Pacific Oceans during concurrent ENSO and IOD events, such as occurred in 2006, has received much recent attention by the numerical modelers [e.g., *Murtugudde et al.*, 1998; *Feng et al.*, 2001; *England and Huang*, 2005; *Potemra and Schneider*, 2007; etc.]. From June 2005 to the end of 2006, the Pacific and Indian wind stresses are correlated and out of phase (Figure 6a), a modulation of the Walker circulation, as also occurred during the concurrent 1997–98 El Niño and IOD events. The partial interannual anticorrelation between Pacific and Indian equatorial zonal winds (exemplified during the 1997/98 co-event and also evident during 2006 in Figure 6a) often results in a partial cancellation of the wind effect on the ITF transport: the Indian easterlies and Pacific westerlies both tend to drop dynamic height in the ITF region, and thus the large-scale pressure gradient driving the ITF is not much affected (T. Lee, personal communication). Further, *Potemra and Schneider*'s [2007] coupled model results show that it is the anomalous local South Java winds that often play a critical role in moderating the total ITF transport during El Niño and IOD events. Thus during the extreme El Niño and IOD events in 1997/98, the reduction in total model ITF transport was smaller than expected because of anomalous easterly winds south of Java that enhanced the upper layer ITF [*Potemra and Schneider*, 2007]. Indeed, during INSTANT, prolonged anomalous easterly winds were found along the south coast

of Java (not shown) from June through December 2006, and it is plausible that these local winds resulted in the elevated ITF transport in the upper layer of all three straits (Figure 6).

[48] During the 2006 IOD, anomalous zonal winds in the equatorial Indian Ocean forced a series of both downwelling and upwelling Kelvin waves with clear sea surface height anomaly (SSHa) signatures [see *Horii et al.*, 2008, Figure 3]. In May 2006, equatorial easterly wind anomalies and the propagation of negative SSHa in the equatorial Indian Ocean coincided with the appearance of coherent anomalously cooler temperatures and eastward currents between 100 and 300 m depth measured at a TRITON buoy located at 0°, 90°E [*Horii et al.*, 2008]. This suggests an upwelling Kelvin wave reached the coastline of Sumatra at 100°E in late May to early June 2006. This was followed 2 months later by a weak downwelling Kelvin wave (westerly wind anomalies and positive SSHa propagation), and a stronger upwelling Kelvin wave 1 month after that, which also had coherent anomalous currents and temperatures signatures observed at the TRITON buoy [*Horii et al.*, 2008]. The INSTANT observations also clearly show a strong reversal of the transport below the thermocline in all three straits (appearing first at depth) that agrees with the timing of the propagation of these Kelvin wave packets from the equatorial region (Figure 6). The anomalous currents associated with the upwelling Kelvin waves in June–July 2006 and September–October 2006 are particularly strong. Similar current reversals and cooler water was associated with the passage of an upwelling Kelvin wave observed at a mooring south of Java during the 1997–98 IOD event [*Sprintall et al.*, 1999]. The INSTANT measurements show that, as found on semiannual timescales, the intraseasonal Kelvin waves propagate even further east along the coastal waveguide. The striking discovery during the INSTANT time period is that the response of the transport anomalies to the 2006 IOD is surprisingly similar in all three exit passages, even in Timor Passage, which being bounded to the Australian shelf, was believed to have a more direct influence from the Pacific equatorial waveguide [*Clarke and Liu*, 1994; *Wijffels and Meyers*, 2004].

4.5. Comparison With Historical Direct Measurements of the ITF

[49] Total transports in each of the exit passages over the INSTANT period agree fairly well with those from previous studies (Table 1). The INSTANT 3-year mean Lombok ITF transport is −2.6 Sv, ranging from −1.8 to −3.2 Sv, compared to the *Murray and Arief* [1988] average transport of −1.7 Sv that was based on an average of the current meter data from either side of the channel. INSTANT clearly shows stronger flow on the western (Bali) side of the channel (Figure 2), that is accounted for in our cross-channel interpolation of the ASV. During the 1985 experiment, the upper layer on the stronger western side of the channel was only instrumented after June 1985, and hence the *Murray and Arief* [1988] annual average transport may be slightly underestimated during the maximum flow of the SEM season.

[50] In Ombai Strait, *Molcard et al.* [2001] found an average ITF transport of −5.0 ± 1.0 Sv for calendar year 1996, derived from a single mooring located very close to our Ombai South INSTANT mooring. This is similar to the mean full-depth transport of −4.9 Sv found during the INSTANT time period, although it is also the upper bound of our transport range from −2.7 Sv to −5 Sv (Table 1). Undoubtedly the observed flow reversals in the northern part of the passage (Figure 2) act to reduce the total ITF through Ombai Strait. It is likely that the severe change in angular momentum of the flow coming around Alor island through Wetar Strait confines the main core of the ITF to the southern part of Ombai Strait, while the Nusa Tenggara coastal waveguide permits the continuous passage of the SJC and SJUC through the Savu Sea hugging the northern walls of Ombai Strait. For the first time, the INSTANT data clearly shows (e.g., Figures 2b and 3b) that both the SJC and SJUC are semipermanent features of the flow through Ombai Strait.

[51] While Ombai Strait carries a significant portion of the full-depth total ITF transport, around half is carried by Timor Passage (−7.5 Sv). Even with a range of possible transports from −6.2 Sv to −10.5 Sv during INSTANT (Table 1), this is still significantly more than the previous estimates of roughly −4.5 Sv found in 1989 [*Molcard et al.*, 1994] and 1992 [*Molcard et al.*, 1996]. The two moorings deployed in 1992 by *Molcard et al.* [1996], which provide the previous "best" estimate of the ITF transport through Timor Passage, were located near to our Timor Sill and Timor South Slope. The large discrepancy between the 1992 and INSTANT period total ITF transport in Timor Passage may be attributed to the missing contribution to the flow by inclusion of the bounding Timor Roti and Timor Ashmore mooring data. In addition, *Molcard et al.* [1996] assumed an 85 km wide Timor Passage in calculating the total transport, whereas our transport accounts for an 160 km wide Passage between Roti Island and Ashmore Reef that permits a significant transport contribution along the southern continental slope of this passage (e.g., Figure 3). Observations reported by *Cresswell et al.* [1993] from the southern part of Timor Passage (Table 1), suggest that the Timor ITF is indeed wide and fills the entire strait.

[52] The earlier direct measurements in the exit passages generally lasted for only a year, hence the 3-year INSTANT deployment provides our best estimate of the seasonal cycle in transport through the exit passages to date (Table 3). Surprisingly the amplitude of the surface-to-sill depth seasonal cycle is relatively small, being only 3 Sv in both Lombok (ranging from −4.3 Sv in August to −1.4 Sv in December) and Timor (−9.0 Sv in April to −6.1 Sv in November). In Ombai Strait, the (0–1200 m) seasonal transport range is 5.5 Sv, ranging from −2.5 Sv in April and −8.0 Sv in December that, as discussed in section 3.4, is totally out of phase with full-depth transport through Timor Passage. For completeness, we also present the amplitude, phase and percent variance explained by the annual and semiannual harmonics that comprise the seasonal cycle in all three exit passages and for the full ITF (Table 4). In the upper 300 m, the seasonal transport at Timor and Lombok is mostly annual and explains ∼20% of the transport variance, although the amplitude of the semiannual harmonic at Lombok is near that found on semiannual timescales in Ombai which has virtually no annual cycle and 14% of the variance is explained by the semiannual cycle (Table 4). Similarly, for the full-depth transport, the annual cycle is dominant in Timor Passage (25% of the

Table 4. Amplitude (Sv), Phase (Days From 1 January) and Percent Variance Explained by the Annual and Semiannual Harmonics of the Seasonal Cycle in Transport Over Various Depth Ranges in Lombok, Ombai, and Timor Passages and the Total Combined Indonesian Throughflow Transport (Lombok 0–300 m, Ombai 0–1200 m, Timor 0–1890 m)

Passage and Depth Range	Annual Amplitude (Sv)	Annual Phase (days)	Annual % Var. Expl	Semiannual Amplitude (Sv)	Semiannual Phase (day)	Semiannual % Var. Expl
Lombok (0–300 m)	1.14	22	18	0.73	128	8
Ombai (0–300 m)	0.26	106	1	0.87	132	14
Timor (0–300 m)	0.85	348	22	0.32	168	3
Ombai (0–1200 m)	0.56	171	1	2.68	90	35
Timor (0–1890 m)	1.45	288	25	0.29	8	1
Total ITF	1.23	319	3	2.67	97	17

variance), while the semiannual cycle dominates full-depth transport through Ombai Strait (35% of the variance). As noted above, the amplitude of both the annual and the semiannual harmonics of transport through each passage are relatively small. The amplitude of the semiannual cycle in Ombai Strait is the same magnitude (2.7 Sv) as that of the semiannual cycle for the full ITF, while the amplitude of the annual cycle for the full ITF (1.2 Sv) is similar to that found in Timor Passage (Table 4). Most of the variance is found at intraseasonal frequencies, for example, 51% of the variance in Ombai Strait is explained by the signal at periods of 30–60 days. The variability in this intraseasonal band is explored further in Wijffels et al. (in preparation).

4.6. Total ITF Mass and Temperature Transports

[53] Total transport through all three passages during the 2004–2006 INSTANT period was −15.0 Sv toward the Indian Ocean, ranging from −10.7 Sv to −18.7 Sv depending on how the missing surface and bottom layers were extrapolated. There are only slight differences in the annual mean transport from year to year: −13.8 Sv in 2004, and −15.4 Sv in both 2005 and 2006. The ITF transports predicted from mean wind stress observations using the *Godfrey* [1989] Island Rule during the INSTANT program were −13.1 to −13.5 Sv using scatterometer-based wind estimates, and therefore within the range of observed transports. The total transport measured through Makassar Strait during INSTANT was −11.6 ± 3.3 Sv [*Gordon et al.*, 2008], and an additional small surface contribution (∼1 Sv) may enter from the South China Sea [*Tozuka et al.*, 2007]. This total inflow of around −12.6 Sv is in general agreement with the −13.3 Sv estimated through the exit passages from the surface to 680 m (the Dewakang Sill depth). Lifamatola Passage, the deeper ITF inflow portal, must contribute the remaining ∼2 Sv of IIW (∼700–1200 m) that exits through the Nusa Tenggara passages, although this depth range was not resolved well by the INSTANT mooring measurements in Lifamatola [*van Aken et al.*, 2009]. Below 1250 m, the average volume transport through Lifamatola during INSTANT was −2.5 ± 1.5 Sv [*van Aken et al.*, 2009]. However, to participate in the ITF this transport must upwell in the Banda Sea or other internal seas, as the deepest controlling sill depth into the Indian Ocean is Leti Strait (∼1250 m) at the eastern end of Timor Passage.

[54] Over the INSTANT period, the TWT of the total ITF export is 17.6°C which is significantly warmer than the 15.6°C TWT of the 11.6 Sv Makassar Strait transport during INSTANT [*Gordon et al.*, 2008]. Export transports in the upper 750 m are −13.5 Sv at 19°C suggesting a temperature increase of ∼3.4°C as the upper ITF transits the Flores and Banda Seas. *Wijffels et al.* [2008] 20-year mean estimates of the upper 750 m geostrophic plus Ekman flow across ITF-intersecting XBT lines agrees reasonably well with the 3-year INSTANT data: 9 Sv at 19.7°C across a line close to the export straits (PX2) and 9 Sv at 21.2°C across a line 1500 km downstream in the Indo-Australian Basin (IX1). Clearly, consistent and significant warming occurs in the ITF as it passes from Makassar Strait through the export straits and into the South Indian Ocean. Local air-sea fluxes are largely able to account for this warming, although the available estimates vary greatly between sources [*Wijffels et al.*, 2008]. A full and detailed mass and heat budget of the internal seas using the INSTANT data set is the topic of future work.

[55] **Acknowledgments.** We sincerely thank the captains and crew of the Baruna Jaya I and VIII for their skilful operations during the three INSTANT research cruises. Support and companionship from Indonesian students from various institutions and scientists from the Indonesian agencies LIPI, BPPT, and BRKP during the cruises are also appreciated. The careful design, deployment, and recovery by mooring engineers and technicians from CSIRO, SIO, and LOCEAN largely contributed to the success of the INSTANT field program. Rebecca Cowley is thanked for her mammoth effort in the quality control of the INSTANT data set. The INSTANT field program and data analysis are funded by the National Science Foundation grants OCE-0220382 and OCE-0725476 (J.S.), Australian Greenhouse Research Program (S.E.W.), and the French Institut des Sciences de l'Univers (projet LEFE; R.M.).

References

Atmadipoera, A., R. Molcard, G. Madec, S. Wijffels, J. Sprintall, A. Koch-Larrouy, I. Jaya, and A. Supangat (2009), Characteristics and variability of the Indonesian Throughflow water at the outflow straits, *Deep Sea Res.*, in press.

Bray, N. A., S. Hautala, J. Chong, and J. Pariwono (1996), Large scale sea level, thermocline, and wind variations in the Indonesian Throughflow region, *J. Geophys. Res.*, *101*, 12,239–12,254.

Clarke, A. J., and X. Liu (1993), Observations and dynamics of semiannual and annual sea levels near the eastern equatorial Indian Ocean boundary, *J. Phys. Oceanogr.*, *23*, 386–399.

Clarke, A. J., and X. Liu (1994), Interannual sea level in the northern and eastern Indian Ocean, *J. Phys. Oceanogr.*, *24*, 1224–1235.

Cowley, R., B. Heaney, S. Wijffels, L. Pender, J. Sprintall, S. Kawamoto, and R. Molcard (2008), INSTANT Sunda Data Report Description and Quality Control. (Available at http://www.marine.csiro.au/∼cow074/INSTANTdataQC_v4.pdf)

Cresswell, G., A. Frische, J. Peterson, and D. Quadfasel (1993), Circulation in the Timor Sea, *J. Geophys. Res.*, *98*, 14,379–14,389.

Dunn, J. R., and K. R. Ridgway (2002), Mapping ocean properties in regions of complex topography, *Deep Sea Res. Part 1*, *49*(3), 591–604.

Durland, T. S., and B. Qiu (2003), Transmission of subinertial Kelvin waves through a strait, *J. Phys. Oceanogr.*, *33*, 1337–1350.

England, M. H., and F. Huang (2005), On the interannual variability of the Indonesian Throughflow and its linkage with ENSO, *J. Clim.*, *18*, 1435–1444.

Feng, M., and S. Wijffels (2002), Intraseasonal variability in the South Equatorial Current of the East Indian Ocean, *J. Phys. Oceanogr.*, *32*, 265–277.

Feng, M., G. Meyers, and S. E. Wijffels (2001), Interannual upper ocean variability in the tropical Indian Ocean, *Geophys. Res. Lett.*, *28*(21), 4151–4154.

Ffield, A., and A. L. Gordon (1992), Vertical mixing in the Indonesian thermocline, *J. Phys. Oceanogr.*, *22*, 184–195.

Ffield, A., K. Vranes, A. L. Gordon, R. D. Susanto, and S. L. Garzoli (2000), Temperature variability within Makassar Strait, *Geophys. Res. Lett.*, *27*, 237–240.

Fieux, M., C. Andrie, P. Delecluse, A. G. Ilahude, A. Kartavtseff, F. Mantisi, R. Molcard, and J. C. Swallow (1994), Measurements within the Pacific-Indian Oceans Throughflow region, *Deep Sea Res., Part I*, *41*, 1091–1130.

Fieux, M., R. Molcard, and A. G. Ilahude (1996), Geostrophic transport of the Pacific-Indian Oceans Throughflow, *J. Geophys. Res.*, *101*, 12,421–12,432.

Godfrey, J. S. (1989), A Sverdrup model of the depth-integrated flow for the world ocean allowing for island circulations, *Geophys. Astrophys. Fluid Dyn.*, *45*, 89–112.

Godfrey, J. S. (1996), The effect of the Indonesian Throughflow on ocean circulation and heat exchange with the atmosphere: A review, *J. Geophys. Res.*, *101*, 12,217–12,237.

Gordon, A. L. (1986), Interocean exchange of thermocline water, *J. Geophys. Res.*, *91*, 5037–5046.

Gordon, A. L., S. Ma, D. B. Olson, P. Hacker, A. Ffield, L. D. Talley, D. Wilson, and M. Baringer (1997), Advection and diffusion of Indonesian Throughflow water within the Indian Ocean South Equatorial Current, *Geophys. Res. Lett.*, *24*, 2573–2576.

Gordon, A. L., R. D. Susanto, and A. Ffield (1999), Throughflow within Makassar Strait, *Geophys. Res. Lett.*, *26*, 3325–3328.

Gordon, A. L., and R. D. Susanto (2001), Banda Sea surface-layer divergence, *Ocean Dyn.*, *52*, 2–10.

Gordon, A. L., R. D. Susanto, A. Ffield, B. A. Huber, W. Pranowo, and S. Wirasantosa (2008), Makassar Strait Throughflow, 2004–2006, *Geophys. Res. Lett.*, *35*, L24605, doi:10.1029/2008GL036372.

Gronell, A., and S. E. Wijffels (2008), A semi-automated approach for quality-controlling large historical ocean temperature archives, *J. Atmos. Ocean. Technol.*, *25*(6), 990–1003.

Hautala, S. L., J. L. Reid, and N. Bray (1996), The distribution and mixing of Pacific water masses in the Indonesian Seas, *J. Geophys. Res.*, *101*, 12,375–12,389.

Hautala, S. L., J. Sprintall, J. Potemra, A. G. Ilahude, J. C. Chong, W. Pandoe, and N. Bray (2001), Velocity structure and transport of the Indonesian Throughflow in the major straits restricting flow into the Indian Ocean, *J. Geophys. Res.*, *106*, 19,527–19,546.

Hirst, A. C., and J. S. Godfrey (1993), The role of the Indonesian Throughflow in a global ocean GCM, *J. Phys. Oceanogr.*, *23*, 1057–1086.

Hirst, A. C., and J. S. Godfrey (1995), The response to a sudden change in the Indonesian Throughflow in a global ocean GCM, *J. Phys. Oceanogr.*, *24*, 1894–1910.

Horii, T., H. Hase, I. Ueki, and Y. Masumoto (2008), Oceanic precondition and evolution of the 2006 Indian Ocean dipole, *Geophys. Res. Lett.*, *35*, L03607, doi:10.1029/2007GL032464.

Hughes, T. M. C., A. J. Weaver, and J. S. Godfrey (1992), Thermohaline forcing of the Indian Ocean by the Pacific Ocean, *Deep Sea Res.*, *39*, 965–995.

Johnson, H. L., and C. Garrett (2006), What fraction of a Kelvin wave incident on a narrow strait is transmitted?, *J. Phys. Oceanogr.*, *36*, 945–954.

Koch-Larrouy, A., G. Madec, D. Iudicone, A. Atmadipoera, and R. Molcard (2008), Physical processes contributing to the water mass transformation of the Indonesian Throughflow, *Ocean Dyn.*, *58*(3), 275–288.

Lee, T., I. Fukumori, D. Menemenlis, Z. Xing, and L. L. Fu (2002), Effects of the Indonesian Throughflow on the Pacific and Indian Oceans, *J. Phys. Oceanogr.*, *32*, 1404–1429.

Masumoto, Y. (2002), Effects of interannual variability in the eastern Indian Ocean on the Indonesian Throughflow, *J. Oceanogr. Jpn.*, *58*, 175–182.

Masumoto, Y., and T. Yamagata (1996), Seasonal variations of the Indonesian Throughflow in a general circulation model, *J. Geophys. Res.*, *101*, 12,287–12,293.

McClean, J. L., D. P. Ivanova, and J. Sprintall (2005), Remote origins of interannual variability in the Indonesian Throughflow region from data and a global Parallel Ocean Program simulation, *J. Geophys. Res.*, *110*, C10013, doi:10.1029/2004JC002477.

McCreary, J. P., Jr. (1984), Equatorial beams, *J. Mar. Res.*, *42*, 395–430.

Meyers, G. (1996), Variation of Indonesian throughflow and the El Niño-Southern Oscillation, *J. Geophys. Res.*, *101*, 12,255–12,263.

Meyers, G., R. J. Bailey, and A. P. Worby (1995), Geostrophic transport of Indonesian throughflow, *Deep Sea Res., Part I*, *42*, 1163–1174.

Molcard, R., A. G. Ilahude, M. Fieux, J. C. Swallow, and J. Banjarnahor (1994), Low frequency variability of the currents in Indonesian Channels (Savu-Roti M1 and Roti-Ashmore Reef M2), *Deep Sea Res.*, *41*, 1643–1662.

Molcard, R. M., M. Fieux, and A. G. Ilahude (1996), The Indo-Pacific Throughflow in the Timor Passage, *J. Geophys. Res.*, *101*, 12,411–12,420.

Molcard, R. M., M. Fieux, and F. Syamsudin (2001), The Throughflow within Ombai Strait, *Deep Sea Res.*, *48*, 1237–1253.

Moore, T. S., II, and J. Marra (2002), Satellite observations of bloom events in the Strait of Ombai: Relationships to monsoons and ENSO, *Geochem. Geophys. Geosyst.*, *3*(2), 1017, doi:10.1029/2001GC000174.

Murray, S. P., and D. Arief (1988), Throughflow into the Indian Ocean through the Lombok Strait, January 1985–January 1986, *Nature*, *333*, 444–447.

Murtugudde, R., A. Busalacchi, and J. Beauchamp (1998), Seasonal to interannual effects of the Indonesian Throughflow on the tropical Indo-Pacific basin, *J. Geophys. Res.*, *103*(C10), 21,425–21,441.

Potemra, J. T. (2001), The potential role of equatorial Pacific winds on southern tropical Indian Ocean Rossby waves, *J. Geophys. Res.*, *106*, 2407–2422.

Potemra, J. T., and N. Schneider (2007), Interannual variations of the Indonesian throughflow, *J. Geophys. Res.*, *112*, C05035, doi:10.1029/2006JC003808.

Potemra, J. T., S. L. Hautala, and J. Sprintall (2003), Vertical structure of the Indonesian Throughflow, *Deep-Sea Res., Part II*, *50*, 2143–2162.

Saji, N. H., B. H. Goswami, P. N. Vinayachandran, and T. Yamagata (1999), A dipole mode in the tropical Indian Ocean, *Nature*, *401*, 360–363.

Schiller, A., J. S. Godfrey, P. C. McIntosh, G. Meyers, and S. E. Wijffels (1998), Seasonal near-surface dynamics and thermodynamics of the Indian Ocean and Indonesian Throughflow in a global ocean general circulation model, *J. Phys. Oceanogr.*, *11*, 2288–2312.

Schneider, N. (1998), The Indonesian throughflow and the global climate system, *J. Climate*, *11*, 676–689.

Song, Q., A. L. Gordon, and M. Visbeck (2004), Spreading of the Indonesian throughflow in the Indian Ocean, *J. Phys. Oceanogr.*, *34*, 772–779.

Smith, W. H. F., and D. T. Sandwell (1997), Global seafloor topography from satellite altimetry and ship depth soundings, *Science*, *277*, 1957–1962.

Sprintall, J., J. Chong, F. Syamsudin, W. Morawitz, S. Hautala, N. Bray, and S. Wijffels (1999), Dynamics of the South Java current in the Indo-Australian Basin, *Geophys. Res. Lett.*, *26*, 2493–2496.

Sprintall, J., A. L. Gordon, R. Murtugudde, and R. D. Susanto (2000), A semiannual Indian Ocean forced Kelvin wave observed in the Indonesian seas in May 1997, *J. Geophys. Res.*, *105*, 17,217–17,230.

Sprintall, J., J. T. Potemra, S. L. Hautala, N. A. Bray, and W. W. Pandoe (2003), Temperature and salinity variability in the exit passages of the Indonesian Throughflow, *Deep Sea Res., Part II*, *50*, 2183–2204.

Sprintall, J., S. Wijffels, A. L. Gordon, A. Ffield, R. Molcard, R. D. Susanto, I. Soesilo, J. Sopaheluwakan, Y. Surachman, and H. M. van Aken (2004), INSTANT: A new international array to measure the indonesian throughflow, *Eos Trans. AGU*, *85*, 369, doi:10.1029/2004EO390002

Talley, L. D., and J. Sprintall (2005), Deep expression of the Indonesian Throughflow: Indonesian intermediate water in the South Equatorial Current, *J. Geophys. Res.*, *110*, C10009, doi:10.1029/2004JC002826.

Tozuka, T., T. Qu, and T. Yamagata (2007), Dramatic impact of the South China Sea on the Indonesian Throughflow, *Geophys. Res. Lett.*, *34*, L12612, doi:10.1029/2007GL030420.

van Aken, H. M., I. S. Brodjonegoro, and I. Jaya (2009), The deep water motion through the Lifamatola Passage and its contribution to the Indonesian Throughflow, *Deep Sea Res.*, doi:10.1016/j.dsr.2009.02.001, in press.

Vinayachandran, P. N., J. Kurian, and C. P. Neema (2007), Indian Ocean response to anomalous conditions in 2006, *Geophys. Res. Lett.*, *34*, L15602, doi:10.1029/2007GL030194.

Warren, B. A. (1981), Transindian hydrographic section at lat. 18°S: Property distribution s and circulation in the south Indian Ocean, *Deep Sea Res., Part A*, *28*, 759–788.

Waworuntu, J. M., R. A. Fine, D. B. Olson, and A. L. Gordon (2000), Recipe for Banda Sea water, *J. Mar. Res.*, *58*, 547–569.

Wijffels, S., and G. Meyers (2004), An intersection of oceanic waveguides: Variability in the Indonesian Throughflow region, *J. Phys. Oceanogr.*, *34*, 1232–1253.

Wijffels, S., J. Sprintall, M. Fieux, and N. Bray (2002), The JADE and WOCE I10/IR6 Throughflow sections in the Southeast Indian Ocean. Part 1: Water mass distribution and variability, *Deep Sea Res., Part II*, *49*, 1341–1362.

Wijffels, S., G. Meyers, and J. S. Godfrey (2008), A Twenty Year Average of the Indonesian Throughflow: Regional currents and the interbasin exchange, *J. Phys. Oceanogr.*, *38*, 1965–1978.

Wyrtki, K. (1973), An equatorial jet in the Indian Ocean, *Science*, *181*, 262–264.

Wyrtki, K. (1987), Indonesian Throughflow and the associated pressure gradient, *J. Geophys. Res.*, *92*, 12,941–12,946.

You, Y. (1998), Intermediate water circulation and ventilation of the Indian Ocean derived from water mass analysis, *J. Mar. Res.*, *56*, 1029–1067.

Yu, L., and M. M. Rienecker (1999), Mechanisms for the Indian Ocean warming during the 1997–1998 El Niño, *Geophys. Res. Lett.*, *26*, 735–738.

I. Jaya, Department of Marine Sciences and Technology, Bogor Agricultural University, Gedung FPIK, Kampus Darmaga, Bogor 16680, Indonesia.

R. Molcard, LOCEAN, Université Pierre et Marie Curie, Tower 45-55, 4th Floor, 4, place Jussieu 75252, Paris Cedex 05, France.

J. Sprintall, Scripps Institution of Oceanography, University of California San Diego, Mail Code 0230, 9500 Gilman Drive, La Jolla, CA 92093-0230, USA. (jsprintall@ucsd.edu)

S. E. Wijffels, Centre for Australian Weather and Climate Research, CSIRO Marine and Atmospheric Research, Castray Esplanade, GPO Box 1538, Hobart, Tas 7000, Australia.